Redox Biology 46 (2021) 102082

Contents lists available at ScienceDirect

Redox Biology

journal homepage: www.elsevier.com/locate/redox

Pharmaceutical targeting of succinate dehydrogenase in fibroblasts controls bleomycin-induced lung fibrosis

Ziwen Wang [a,g,1], Long Chen [a,1], Yu Huang [a,b,1], Min Luo [a,b], Huilan Wang [a,c], Zhongyong Jiang [a], Jiancheng Zheng [a], Zeyu Yang [d], Zelin Chen [a], Chi Zhang [a], Lei Long [a], Yawei Wang [a], Xueru Li [e], Fengying Liao [a], Yibo Gan [a], Peng Luo [a], Yunsheng Liu [a], Yu Wang [a], XuTan [a], Ziyuan Zhou [f,***], Aihua Zhang [b,**], Chunmeng Shi [a,*]

[a] Institute of Rocket Force Medicine, State Key Laboratory of Trauma, Burns and Combined Injury, Third Military Medical University (Army Medical University), Chongqing, 400038, China
[b] Key Laboratory of Environmental Pollution Monitoring and Disease Control, Ministry of Education, Department of Toxicology, Guizhou Medical University, Guiyang, 550025, China
[c] Institute of Clinical Medicine, Southwest Medical University, Luzhou, 646000, China
[d] Breast and Thyroid Surgical Department, Chongqing General Hospital, University of Chinese Academy of Sciences, Chongqing, 401147, China
[e] Department of Ophthalmology, Third Affiliated Hospital of Chongqing Medical University (Gener Hospital), Chongqing, 401120, China
[f] Department of Environmental Health, College of Preventive Medicine, Third Military Medical University, Chongqing, 400038, China
[g] Department of Cardiology, Geriatric Cardiovascular Disease Research and Treatment Center, The 82nd Group Army Hospital of PLA (252 Hospital of PLA), Baoding, Hebei, 071000, China

ARTICLE INFO

Keywords:
Idiopathic pulmonary fibrosis
Metabolic dysregulation
Succinate
IR-780
Succinate dehydrogenase

ABSTRACT

Idiopathic pulmonary fibrosis (IPF) is characterized by excessive deposition of extracellular matrix in the lung with fibroblast-to-myofibroblast transition, leading to chronically compromising lung function and death. However, very little is known about the metabolic alterations of fibroblasts in IPF, and there is still a lack of pharmaceutical agents to target the metabolic dysregulation. Here we show a glycolysis upregulation and fatty acid oxidation (FAO) downregulation in fibroblasts from fibrotic lung, and perturbation of glycolysis and FAO affects fibroblasts transdifferentiation. In addition, there is a significant accumulation of succinate both in fibrotic lung tissues and myofibroblasts, where succinate dehydrogenase (SDH) operates in reverse by reducing fumarate to succinate. Then succinate contributes to glycolysis upregulation and FAO downregulation by stabilizing HIF-1α, which promotes the development of lung fibrosis. In addition, we identify a near-infrared small molecule dye, IR-780, as a targeting agent which stimulates mild inhibition of succinate dehydrogenase subunit A (SDHA) in fibroblasts, and which inhibits TGF-β1 induced SDH and succinate elevation, then to prevent fibrosis formation and respiratory dysfunction. Further, enhanced cell retention of IR-780 is shown to promote severe inhibition of SDHA in myofibroblasts, which may contribute to excessive ROS generation and selectively induces myofibroblasts to apoptosis, and then therapeutically improves established lung fibrosis in vivo. These findings indicate that targeting metabolic dysregulation has significant implications for therapies aimed at lung fibrosis and succinate dehydrogenase is an exciting new therapeutic target to treat IPF.

Abbreviations: IPF, Idiopathic pulmonary fibrosis; FAO, Fatty acid oxidation; SDH, Succinate dehydrogenase; ECM, Excessive extracellular matrix; α-SMA, Alpha-smooth muscle actin; ECAR, Extracellular acidification rate; OCR, Oxygen consumption rate; NIR, Near-infrared; OATPs, Organic-anion-transporting polypeptide; SLC, Solute carrier family; TEM, Transmission electron microscopy; BALF, Bronchoalveolar Lavage Fluid.

* Corresponding author
** Corresponding author
*** Corresponding author
E-mail addresses: ziyuanzhou@tmmu.edu.cn (Z. Zhou), aihuagzykd@163.com (A. Zhang), shicm@sina.com (C. Shi).
[1] These authors contributed equally to this work.

https://doi.org/10.1016/j.redox.2021.102082
Received 13 May 2021; Accepted 23 July 2021
Available online 26 July 2021

1. Introduction

Idiopathic pulmonary fibrosis (IPF), a fatal and progressive fibrosing parenchymal respiratory disorder of unknown etiology [1], is the most serious prognosis of non-cancer related lung diseases with a high prevalence [2]. Even worse, the COVID-19 pandemic further aggravates the IPF burden because of the similar risk factors [3]. IPF reveals the replacement of normal alveoli by fibrous scars containing excessive extracellular matrix (ECM) protein [4,5], the fibroblast-to-myofibroblast transition is a key step in IPF and myofibroblasts are considered to be the predominant effector of ECM homeostasis, presenting a highly contractile and synthetic profile in IPF [5,6]. Therefore, inhibiting fibroblast transition or targeting apoptosis of myofibroblasts can be a therapeutic strategy to ameliorate lung fibrosis.

IPF involves multiple mediators acting through an interactive network of signaling pathways to regulate fibroblasts. Metabolism is essential to all cellular functions, and various upstream signaling pathways may converge on key metabolic changes that ultimately regulate phenotypes [7,8]. Alteration in cellular metabolism, including glycolysis and fatty acid oxidation (FAO), has emerged as an important mechanism of various pathological processes, especially in the context of stem cells, carcinogenesis and inflammation [9]. However, very little is known about the alterations of glycolysis and FAO in lung fibroblast transition, and whether metabolic perturbation affects lung fibrosis remains unclear.

Here we show that FAO downregulation and glycolysis upregulation can govern the lung fibroblast behavior, and succinate contributes to metabolic dysregulation by stabilizing HIF-1α. Then we identify a near-infrared small molecule dye, IR-780, as a targeting agent to prevent fibrosis and respiratory dysfunction by suppressing glycolysis and promoting FAO via mild inhibition of succinate dehydrogenase subunit A (SDHA) in fibroblasts. Furthermore, enhanced cell retention of IR-780 is shown to promote severe inhibition of SDHA in myofibroblasts, which may contribute to excessive ROS and selectively induces myofibroblasts to apoptosis, and then therapeutically improves established lung fibrosis in vivo. These findings suggest the importance of targeting glycolysis and FAO disorders to control lung fibrosis and succinate dehydrogenase is a promising target to treat IPF.

2. Results

2.1. Metabolic alterations correspond to lung fibrosis

Altering glycolysis and fatty acid oxidation (FAO) metabolism has been implicated in the various pathological process [10,11], but the alterations in lung fibrosis are not well understood. To uncover the glycolysis and FAO alterations in lung fibrosis, lung fibroblasts were isolated from healthy control and bleomycin-challenged rats. We found fibroblasts from fibrotic lung expressed high levels of myofibroblast markers such as alpha-smooth muscle actin (α-SMA), fibronectin and collagen 1 (Fig. 1A and Fig. S1A), indicating the occurrence of phenotype changes from fibroblast to myofibroblast. Meanwhile, differentiation of fibroblasts to myofibroblasts is associated with increased expression of α-SMA stress fibers resulting in a hyper-proliferative phenotype [12,13], we assessed the proliferation of primary lung fibroblasts isolated from control and fibrotic lung, and the fibroblasts from bleomycin-treated lung had the increasing proliferative ability (Fig. S1B). The mRNAs levels of proliferation specific AURKB, CCNB, CDC25B, and FOXOM1 genes were all increased in fibroblasts isolated from the fibrotic lungs (Fig. S1C).

By using real-time quantitative PCR (RT-qPCR) and immunoblot analysis, we confirmed the downregulation of PPAR signaling (PPARA and PPARG) and their co-activators (PGC1A and PGC1B), and downstream targets ACOX1 and CPT1A, which catalyze rate-limiting steps of fatty acid oxidation (Fig. 1B and C). Inversely, we found the upregulation of key glycolysis enzyme at multiple steps, including upregulation of hexokinase 1 (HK1) and HK2, glucose transporter 1 (GLUT1) and GLUT3, and phosphofructokinase 1 (PFK1) and PFK2 (Fig. 1B and C). Furthermore, the downregulation of key FAO regulators was associated with higher lipid accumulation and triglyceride abundance in the fibrotic lung (Fig. 1D and E). Similarly, flow cytometry-based quantification of LipidTOX^{+} fibroblasts displayed a significant 5-fold increase in lung fibrosis compared with healthy control (Fig. 1F), and we observed considerable accumulation of intracellular lipids in fibroblasts from fibrotic lung (Fig. 1G). Meanwhile, pyruvate kinase M1/2 (PKM2) expression and lactate production were obviously upregulated in fibrotic lung tissues (Fig. 1H and I), and fibroblasts from fibrotic lung showed increased glucose consumption because of hyperglycolysis (Fig. 1J).

For quantitative analysis of metabolism, extracellular acidification rate (ECAR) and oxygen consumption (OCR) of primary fibroblasts were examined. The OCR of fibroblasts from the fibrotic lung was decreased with the addition of fatty acid palmitate and was less sensitive to CPT1A inhibitor (etomoxir) compared with healthy control, indicating a lower level of FAO in lung fibrosis (Fig. 1K). However, the basal glycolysis rate and glycolytic capacity were both increased in fibroblasts from fibrotic lung (Figure 1L). At the same time, primary lung fibroblasts were exposed to hypoxia, TGF-β1 or PDGF-BB, which are reported to promote fibrosis primarily through HIF-1α, SMAD and MEK-ERK signaling, respectively [14,15]. All three mediators increased the expression of myofibroblast parameters: α-SMA, fibronectin and collagen-1 (Fig. S1D). We also observed FAO downregulation and glycolysis upregulation at mRNA and protein levels in all three mediators-induced fibrosis, which is consistent with fibroblasts from fibrotic lung (Figure 1M and Figs. S1E–G). Further, because metabolic reprogramming is usually associated with changes in mitochondrial dynamics, and we found there is a lowered level of relative mitochondrial DNA and a decreased mRNA level of several mitochondrial enzymes and transcription factors in TGF-β1 treated human fetal lung fibroblast cell lines (HFL1) compared to controls (Fig. S1H). In summary, there is a downregulation of FAO and upregulation of glycolysis in fibroblasts correspond to the development of lung fibrosis.

2.2. Perturbation of glycolysis and FAO affects the fibroblast-to-myofibroblast transition

To demonstrate that these metabolic changes have a direct effect on fibroblast phenotype and ECM protein levels, we altered the metabolic condition of lung fibroblasts by inhibiting glycolysis and FAO, respectively (Fig. 2A). Inhibition of glycolysis in primary lung fibroblasts by preventing glucose transporters using BAY876, or by inhibiting hexokinase through 2-DG, or by preventing PFKFB3 using 3-PO, or by knockdown of HK1, downregulated myofibroblast phenotype (Fig. 2B–C and Fig. S2A). Conversely, suppression of FAO by using CPT1 inhibitor etomoxir, or through knockdown of PPARG and CPT1A, resulted in an elevation in myofibroblast parameters (Fig. 2C–D and Fig. S2B). Meanwhile, glycolysis meets the metabolic requirements of cell proliferation and plays a fundamental role in supporting cell growth in the development of fibrosis [16], and as expected, glycolysis inhibition downregulates the proliferation of TGF-β1 induced fibroblasts compared with the normal fibroblasts (Fig. S2C). Next, we examined the effect of the fenofibrate (a PPARA agonist), and we found fenofibrate mitigated TGF-β1-induced fibroblast transdifferentiation (Fig. 2C and E), which suggests that enhancing FAO reduces the fibroblast-to-myofibroblast transition. Meanwhile, FAO and glycolysis were both inhibited in order to figure out the relationship between them, and etomoxir failed to reverse the effect of 2-DG and 3-PO in reducing myofibroblast phenotype (Fig. 2F), which demonstrates that primary inhibition of glycolysis is important to downregulate myofibroblast parameters, and may at least in part, independent of FAO. Suggesting it is crucial and efficient to control lung fibrosis by both inhibiting glycolysis and promoting FAO.

Moreover, it has been proposed that excess lipid accumulation leads

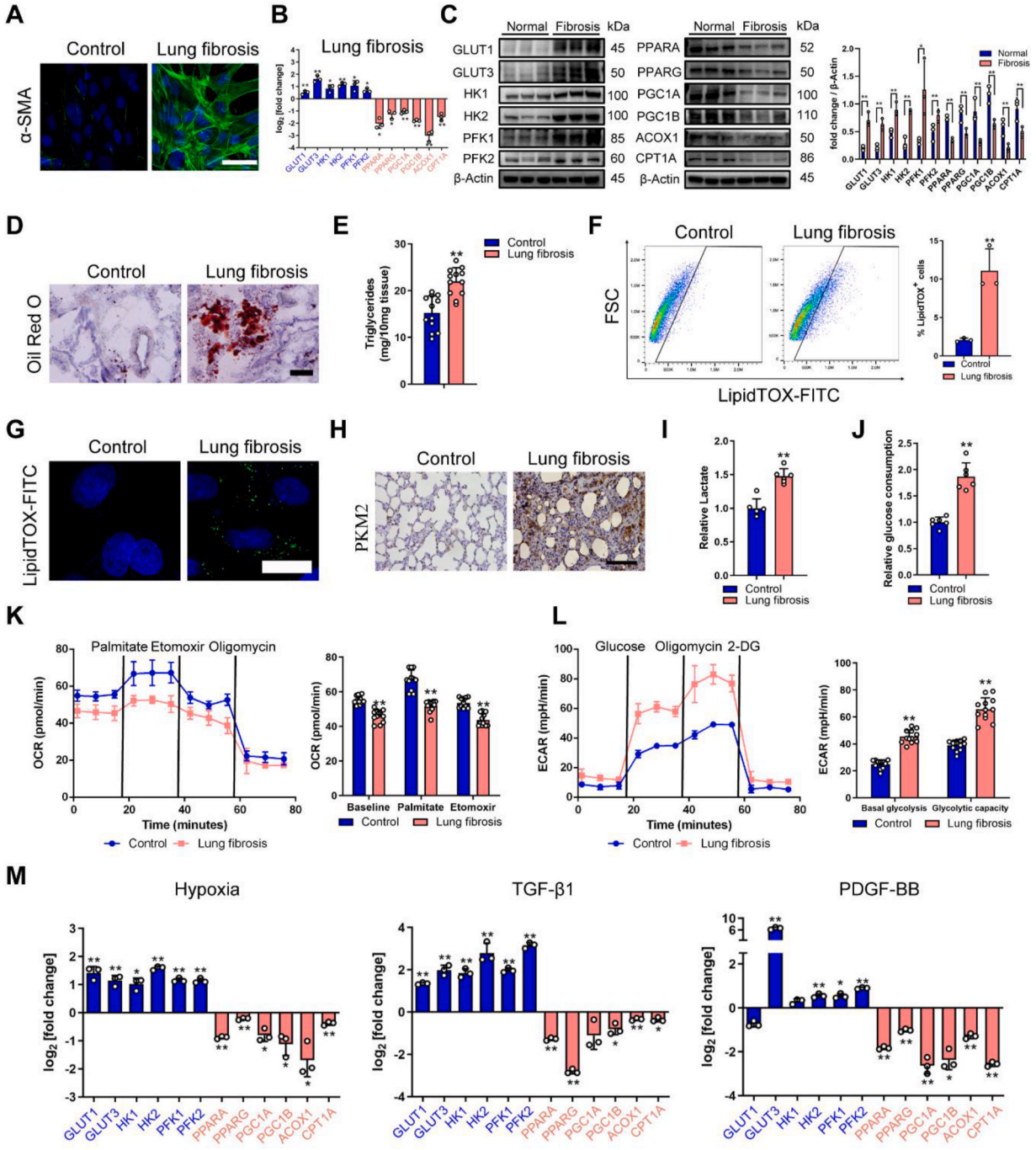

Fig. 1. Downregulation of FAO and upregulation of glycolysis in lung fibrosis. **A** Representative image showing α-SMA (green) and nuclei (blue) in rat fibroblasts from healthy and fibrotic lung (cells were isolated from SD rats after 28 days of PBS or bleomycin treatment). **B** FAO and glycolysis gene transcription alterations in rat fibroblasts from normal and fibrotic lung. mRNA levels of FAO and glycolysis genes are relative to healthy control (n = 3). **C** Western blot analysis of FAO and glycolysis protein in rat fibroblast from the groups indicated. **D** Representative images of Oil Red O staining of lung samples from healthy control and fibrotic lung. **E** Triglyceride abundance in the rat lung tissues indicated (n = 12). **F** Gating strategy for detecting LipidTOX $^{+}$ cells by flow cytometry and quantification of LipidTOX $^{+}$ cell abundance in rat fibroblast from healthy and fibrotic lung (n = 3). **G** Staining of lipid droplets in fibroblasts using LipidTOX (green). Nuclei were counterstained with DAPI (blue). **H** PKM2 staining of lung sections from the groups indicated. **I** Relative lactate production of lung sections from the groups indicated (n = 6). **J** Glucose consumption in rat fibroblast from healthy and fibrotic lung (n = 6). **K** Fatty acid oxidation (n = 4) in rat fibroblast from the healthy and fibrotic lung. Y-axis represents the oxygen consumption rate (OCR), a measure of metabolite oxidation over time. Palmitate (170μM), etomoxir (40μM) and oligomycin (2 μM). Etomoxir inhibits FAO by irreversibly binding to CPT-1A, which catalyzed the transport of fatty acids, such as palmitate, into the mitochondria for β-oxidation. **L** Glycolysis stress test (n = 4) in rat fibroblast from the healthy and fibrotic lung. Y-axis plots the extracellular acidification rate (ECR) which is a measure of glycolysis via the production of lactic acid. Glucose (10 mM), oligomycin (1 μM), and 2-DG (2-Deoxy-Glucose, 100 mM). ECAR, prior to glucose injection, is referred to as non-glycolytic acidification which is caused by other processes rather than glycolysis, and glucose-induced response is reported as the rate of glycolysis under basal conditions. **M** qRT-PCR of FAO and glycolysis genes are relative to control (n = 3). In vitro profiling of primary lung fibroblast with hypoxia (2 %), TGF-β1(5 ng/ml), and PGDF-BB (5 ng/ml). Bars represent 50 μm **(A)**, 125 μm **(D)**, 25 μm **(G)**, 200 μm **(H)**. The results are presented as the means ± S.D. (*p < 0.05, **P < 0.01; student's t-test). (For interpretation of the references to color in this figure legend, the reader is referred to the Web version of this article.)

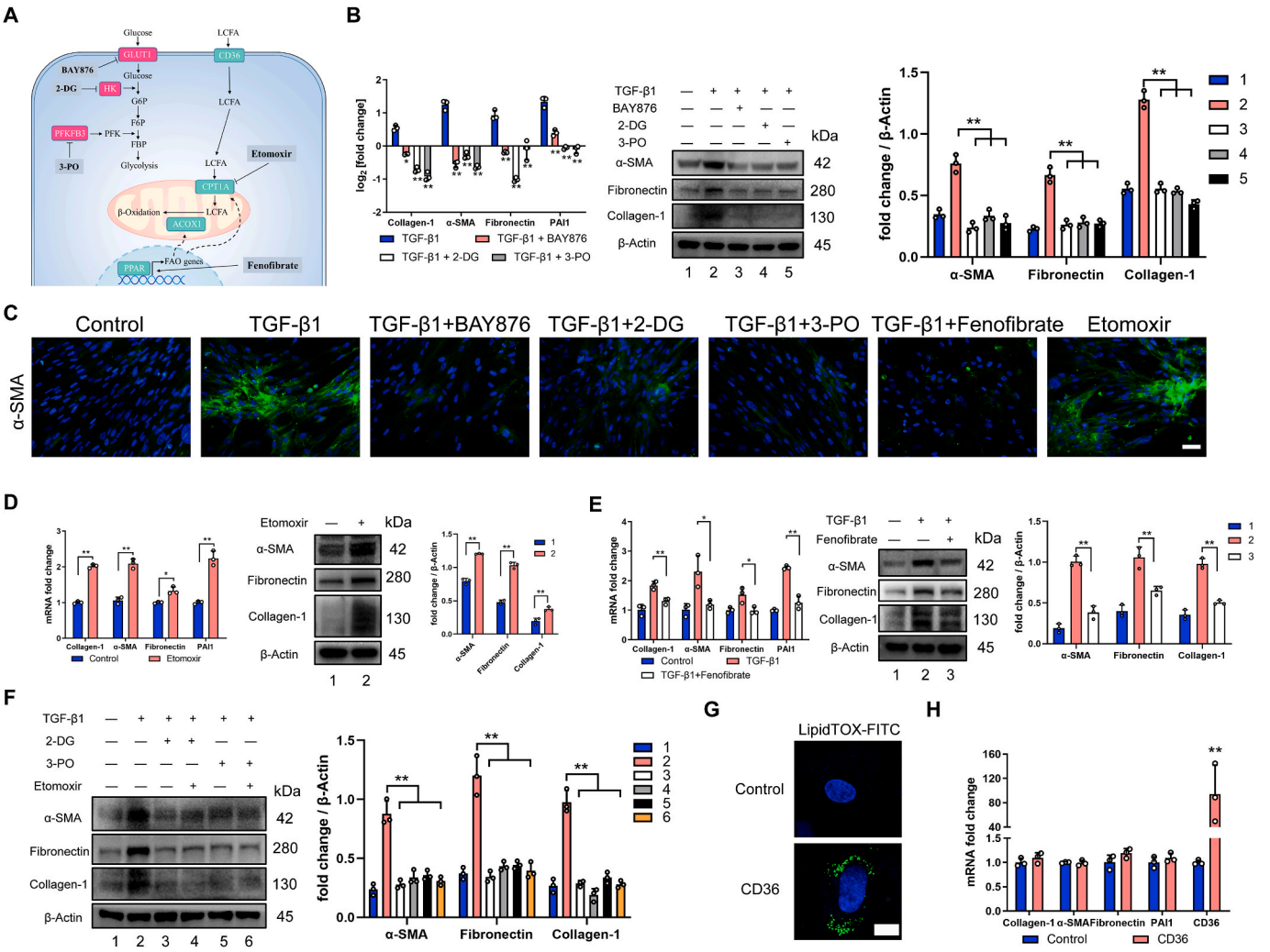

Fig. 2. Perturbation of glycolysis and FAO affects fibroblast-to-myofibroblast transition. **A** Cellular map of metabolic enzymes and pathways targeted by drugs. **B** Inhibiting glycolysis downregulates profibrotic mRNA and protein levels in primary lung fibroblasts. qRT-PCR and Western blot analysis of profibrotic genes and protein (n = 3). **C** Representative image showing α-SMA (green) and nuclei (blue) in primary lung fibroblasts with indicated treatment for 24 h. **D** Inhibiting FAO upregulates profibrotic mRNA and protein levels in primary lung fibroblasts. Relative mRNA and protein levels of profibrotic markers in primary lung fibroblasts treated with etomoxir determined by qRT-PCR and Western blot (n = 3). **E** Relative mRNA and protein levels related to fibrosis in primary lung fibroblast treated with or without TGF-β1 and fenofibrate (n = 3). **F** Representative expressions of profibrotic proteins in primary lung fibroblast with indicated treatment. **G** Staining of lipid droplets using LipidTOX (green) in control HFL1 or cells overexpressed CD36, nuclei were counterstained with DAPI (blue). **H** Relative mRNA expression of transcripts related to fibrosis in control HFL1 or cells overexpressed CD36 (n = 3). Drug doses: TGF-β1 (5 ng/ml), BAY-876 (2.5 μM), 3-PO (5 mM), 2-DG (5 mM), etomoxir (10 μM), fenofibrate (1 μM). Bars represent 100 μm **(C)**, 10 μm **(G)**. The results are presented as the means ± S.D. (*p < 0.05, **P < 0.01; D and H, student's t-test; B and E, One-way ANOVA). (For interpretation of the references to color in this figure legend, the reader is referred to the Web version of this article.)

to the development of fibrosis and lipotoxicity [17]. CD36 can imports long-chain fatty acids (LCFA) intracellularly for FAO [18]. To examine whether lipid accumulation can promote the development of lung fibrosis, we overexpressed human CD36 in human fetal lung fibroblast cell lines (HFL1) which can induce accumulation of intracellular lipids (Fig. 2G). However, quantitative analysis showed little evidence of profibrotic markers in fibroblasts which overexpressed CD36 (Fig. 2H). More interestingly, we found a significant decrease of CD36 expression in fibroblast from fibrotic lung at mRNA and protein level (Fig. S2D), and so do primary lung fibroblasts exposed to three mediators (Hypoxia, TGF-β1 or PDGF-BB) (Figs. S2E–G), this is most probably because that CD36 connects the capacity for collagen internalization and degradation [19], and downregulation of CD36 accounts for the collagen accumulation in lung fibrosis. Therefore, we speculated that reduced FAO could be a major inciting factor for the development of fibrosis and lipid accumulation occurred as a secondary consequence. Taken together, these results show that the enhancement of FAO and inhibition of glycolysis can inhibit fibroblast transdifferentiation effectively.

2.3. *Succinate contributes to metabolic dysregulation in lung fibrosis*

Hypoxia has long been implicated in the pathogenesis of chronic tissue injury and fibrotic diseases [20–22]. It is also well recognized that HIF-1α is the master regulator of glycolytic enzymes expression and the key transcriptional factor which drives glycolysis under hypoxic conditions [23–25]. Meanwhile, HIF-1α can drive lipid deposition and cancer progression via suppression of fatty acid oxidation [26,27]. However, whether HIF-1α can regulate FAO and glycolysis in pulmonary fibrosis remains unclear. In our research, fibroblast from fibrotic lung showed increased HIF-1α protein level but not mRNA expression (Fig. 3A), we also observed a significant increase of HIF-1α in fibrotic lung tissues at the histological level (Fig. 3B). Similarly, TGF-β1 can promote the protein level of HIF-1α (Fig. S3A). Meanwhile, pre-treating TGF-β1 stimulated primary lung fibroblast with a cell-permeable

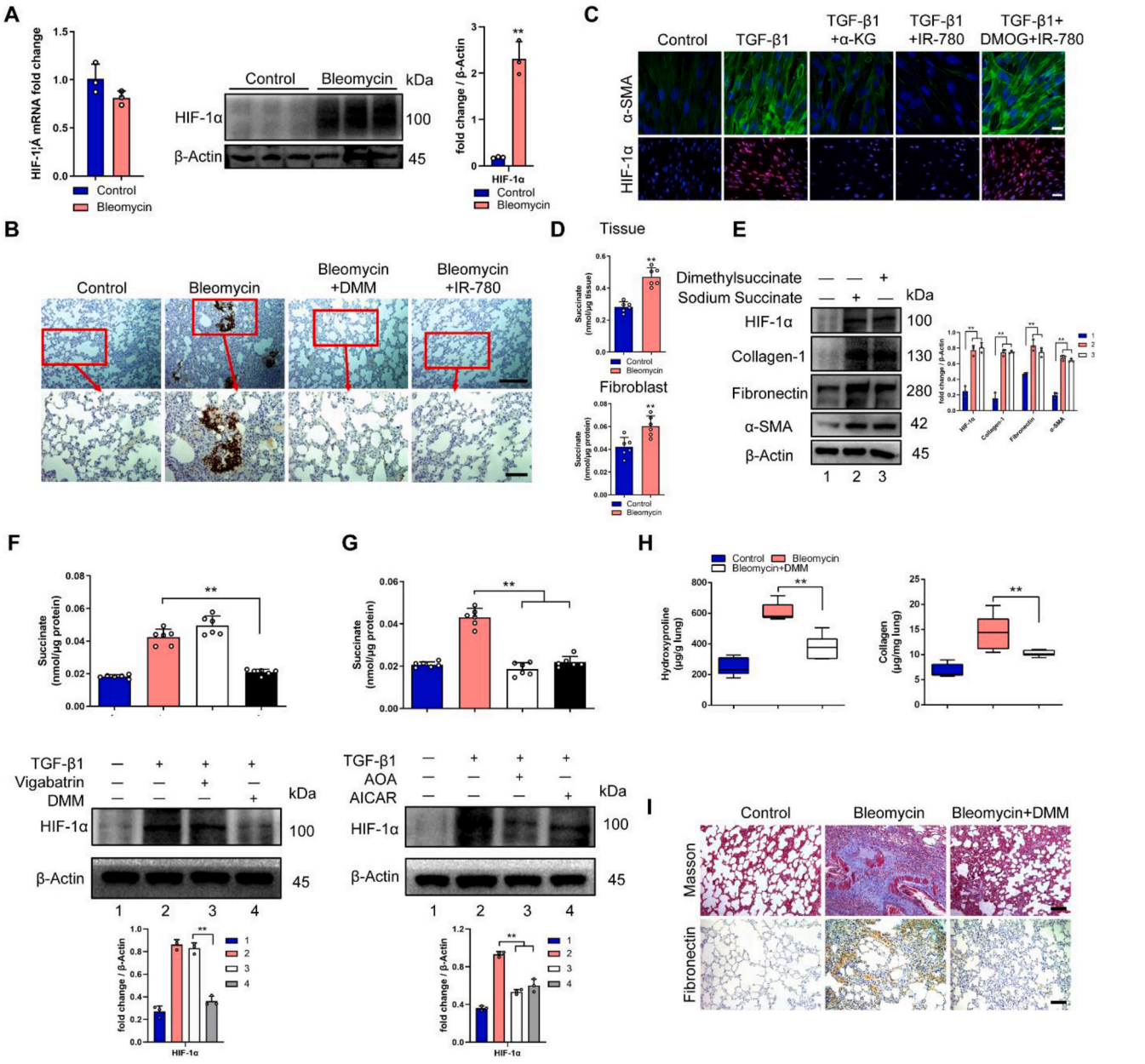

Fig. 3. Succinate contributes to metabolic dysregulation in lung fibrosis. **A** Relative mRNA and protein levels of HIF-1α in rat fibroblast from the groups indicated (n = 3), and cells were isolated from SD rats after 28 days of PBS or bleomycin treatment. **B** Immunohistochemistry analysis of representative rat lung tissue samples showing HIF-1α expression. **C** Representative image showing α-SMA (green), HIF-1α (red) and nuclei (blue) in primary lung fibroblast treated with or without TGF-β1, α-KG, IR-780 and DMOG for 24 h. **D** Succinate abundance in lung tissues and fibroblasts from the groups indicated (n = 6), tissues or cells were isolated from SD rats after 28 days of PBS or bleomycin treatment. **E** Western blot analysis of profibrotic proteins in primary lung fibroblast treated with or without dimethyl succinate and sodium succinate. **F** Succinate abundance and HIF-1α expression in primary lung fibroblast treated with or without TGF-β1, vigabatrin and DMM (n = 6) for 24 h. **G** Succinate abundance and HIF-1α expression in primary lung fibroblast treated with or without TGF-β1, AOA and AICAR for 24 h (n = 6). **H** Hydroxyproline (n = 6) and collagen abundance (n = 12) in the rat lung tissues indicated. **I** Masson's trichrome and immunohistochemistry staining of fibronectin from representative lung sections. Drug doses: TGF-β1 (5 ng/ml), α-KG (1 mM), IR-780 (0.5 μM), DMOG (200 μM), dimethylsuccinate (5 mM), sodium succinate (2 mM), vigabatrin (500 μM), DMM (5 mM), AOA (1 mM) and AICAR (1 mM). Bars represent 200 μm **(B, top)**, 5 μm **(B, bottom)**, 20 μm **(C, top)**, 100 μm **(C, bottom)**, 100 μm **(I)**. The results are presented as the means ± S.D. (**P < 0.01; A and D, student's t-test; F, G and H, One-way ANOVA). (For interpretation of the references to color in this figure legend, the reader is referred to the Web version of this article.)

α-ketoglutarate (α-KG) derivative, which increases PHD activity, can deplete HIF-1α and significantly reverse TGF-β1 induced glycolysis upregulation and PPAR signaling inhibition (Fig. S3A), as well as the myofibroblast phenotype when HIF-1α was suppressed by α-KG (Fig. 3C and Fig. S3B). As assessed by flow cytometry, the LipidTOX^{+} cells displayed a significant decrease when α-KG was applied in TGF-β1 treated fibroblast (Fig. S3C). Glucose consumption returned to normal level when HIF-1α was inhibited by α-KG in TGF-β1 treated fibroblast (Fig. S3D). Besides, α-KG alone cannot influence the parameters of fibrosis, glycolysis, and FAO levels in normal fibroblasts since α-KG may have many metabolic effects in addition to increasing PHD activity (Figs. S3E–F), nor does α-KG affect the cell viability of normal fibroblast (Fig. S3G). These results implicated that HIF-1α is responsible for the metabolic alterations in lung fibrosis and inhibiting HIF-1α can be a therapeutic target in ameliorating lung fibrosis.

In addition, succinate can be transported from mitochondria to

cytoplasm via dicarboxylic acid transporters, where excess succinate can disrupt PHD activity, leading to the stabilization and activation of HIF-1α [28,29]. Notably, the succinate accumulated both in fibrotic lung tissues and myofibroblasts (Fig. 3D). To investigate whether succinate can induce the activation of fibroblast, cells were treated with sodium succinate or dimethyl succinate, and we found a significant increase of HIF-1α expression and myofibroblast phenotype (Fig. 3E), the LipidTOX$^+$ cells displayed a significant increase when treated with dimethyl succinate (Fig. S3C). Considering succinate also has metabolic effects other than just affecting PHD, we evaluated whether succinate still can promote myofibroblast phenotype when cells were treated with α-KG, and we found succinate cannot induce the activation of fibroblast in the presence of α-KG (Fig. S3H). Hence, succinate affects fibroblast-to-myofibroblast transition by activating HIF-1α.

Then, we try to identify the mechanisms responsible for succinate accumulation during fibrosis. In mammalian tissues, succinate is produced by the mitochondrial citric acid cycle (CAC), which is oxidized from GABA (γ-aminobutyric acid) and carbon including glucose, fatty acids and glutamate [28,30]. However, inhibition of the GABA pathway with vigabatrin did not decrease TGF-β1 induced succinate accumulation (Fig. 3F). Instead, dimethyl malonate (DMM), a permeable membrane precursor of SDH competitive inhibitor, can prevent HIF-1α expression and act in reverse to inhibit succinate production (Fig. 3F). SDH has been reported to possess bi-directional catalysis function in the process of succinate to fumarate, and although SDH reversal has not been confirmed in lung fibrosis, earlier speculations suggest that SDH might play an opposite role in anaerobic metabolism by reducing fumarate to succinate, and the accumulation of ischemic succinate was induced by the reversal of SDH [31–34]. The SDH reversal model predicts that the supply of fumarate to succinate comes from two converging pathways: the malate/aspartate pathway and AMP-dependent activation of the purine nucleotide cycle that drives fumarate and succinate production [33,35–38]. We also found increased AMP, fumarate, malate, and NADH/NAD+ in fibroblasts from fibrotic lung tissues and TGF-β1 treated fibroblasts (Figs. S3I–J). In addition, AOA and AICAR could limit the production of succinate and HIF-1α expression in TGF-β1 treated fibroblasts effectively (Fig. 3G). Besides, TGF-β1 treated fibroblasts still showed an increased level of fumarate in the presence of DMM (Fig. S3K). Moreover, fumarate can promote the production of succinate in TGF-β1 treated fibroblast (Fig. S3L). Therefore, fumarate can be an upstream signaling molecule of SDH and succinate. What's more, dimethyl malonate significantly decreased HIF-1α expression in lung tissues (Fig. 3B) with remarkably mitigated pulmonary fibrosis as demonstrated by lower levels of lung hydroxyproline, collagen, fibronectin and weaker Masson's trichrome staining (Fig. 3H and I). Therefore, SDH operates in reverse to produce succinate in the development of lung fibrosis and succinate inhibition could prevent fibrosis in lung.

2.4. IR-780 inhibits glycolysis and promotes FAO by targeting succinate dehydrogenase

Based on the above, pharmacological perturbation of fibroblasts metabolism may reduce pulmonary fibrosis. Our group have established a library of small molecules that consists of mitochondria-targeting near-infrared (NIR) heptamethine dyes [39], imaging in this region is superior to visible wavelengths due to its deep tissue penetration, low background interference, low spontaneous fluorescence and reduced photon scattering [40,41]. We employed the most widely utilized and well-characterized bleomycin-induced pulmonary fibrosis rat model to screen the selective and effective anti-fibrosis agents. Among the molecules tested, we identified IR-780 displayed targeting property in bleomycin-treated lung with low background interfering fluorescence (Fig. 4A). IR-780 is a representative heptamethine cyanine dye with unique NIR optical imaging and therapeutic properties, and it has a heptamethine core with its lipophilic cationic property which is essential for mitochondrial targeting and imaging. We initially described the unique mitochondria-targeting property of IR-780 dye in cells, along with its biocompatible and optical properties [42,43]. In this study, we further demonstrated for the first time the preferential lung accumulation of IR-780 by comparing the fluorescent intensity of the dissected organs (Fig. 4B and C). Next, we labeled fibroblasts and alveolar type II cells by using vimentin and SFTPC, respectively, and we found IR-780 predominantly accumulated in fibroblasts (Fig. 4D). These results indicated that IR-780 selectively accumulate into damaged lung tissues and fibroblast with excellent optical properties for cell imaging and tracking in vivo.

Meanwhile, IR-780 upregulated FAO and downregulated glycolysis mRNA and protein levels (Fig. 4E and Fig. S4A) with enhanced FAO and suppressed glycolysis functionally in TGF-β1 treated primary fibroblasts (Fig. 4F and G). Meanwhile, IR-780 could downregulate the proliferation of TGF-β1 induced fibroblasts compared with normal fibroblasts (Fig. S2C). LipidTOX$^+$ cells and glucose consumption with lactate production were decreased when treated with IR-780 (Fig. 4H–J). IR-780 also markedly inhibited the myofibroblasts parameters (Figs. S4B–C and Fig. 3C), however, these effects were inhibited by the PHD inhibitor DMOG which can stabilize HIF-1α protein (Figs. S4B–C and Fig. 3C). Notably, IR-780 prevented accumulation of succinate in fibroblasts (Fig. 5A), and dimethyl succinate could also abrogate the inhibition of succinate abundance and myofibroblast phenotype (Fig. 5A and Fig. S4D), demonstrating that downregulation of HIF-1α and succinate were necessary for IR-780 to maintain metabolic homeostasis and reduce pro-fibrotic levels.

We have suggested that SDH could operate in reverse to promote the development of lung fibrosis, considering IR-780 preferentially localized in the mitochondria of lung fibroblast (Fig. 5B), and this kind of NIR small molecules can target and inhibit mitochondrial protein, especially mitochondrial complex proteins [39,44]. Therefore, we assumed that IR-780 could inhibit SDH (mitochondrial complex II) activity, and the results were concordant with our hypothesis (Fig. 5C). SDH consists of 2 hydrophilic subunits (SDHA and SDHB) and 2 hydrophobic membrane anchor subunits (SDHC and SDHD). We found a significant decrease of SDHA protein expression among the 4 subunits (Fig. 5D), but without influence on the mRNA level of SDHA (Fig. 5E). Next, to better understand the mechanisms of IR-780 in mediating an anti-fibrotic effect, primary lung fibroblasts were transfected with SDHA expressing plasmid, then cells were treated with IR-780 (0.5 μM) and TGF-β1, and we found IR-780 cannot inhibit SDH activity and downregulate succinate abundance (Fig. S4E), then, we found the ability of inhibiting HIF-1α protein and pro-fibrotic protein abundance by IR-780 (0.5 μM) was vanished (Fig. 5F). These results suggest that IR-780 can promote an anti-fibrotic effect by inhibiting SDHA protein.

Taking advantage of the intrinsic NIR fluorescent properties, the probably interacted proteins of IR-780 were separated by SDS-PAGE (sodium dodecyl sulfate polyacrylamide gel electrophoresis). The NIR fluorescent proteins were subjected to liquid chromatography tandem mass spectrometry identification (LC-MS/MS), and SDHA protein is characterized as one candidate binding protein of IR-780 (source data of LC-MS/MS). Then, IR-780 and SDHA protein were co-stained by immunofluorescence, and the result showed a strong colocalization in lung fibroblasts (Fig. 5G). We next observed SDHA antibody could pull down proteins that labeled with NIR fluorescence in IR-780 treated lung fibroblasts by using pull down assay and SDS-PAGE (Fig. 5H), and we also confirmed that the NIR fluorescence protein was SDHA by applying western-blot analysis (Fig. 5H). Western-blot analysis showed that recombinant human SDHA protein can be cleaved into several fragments by IR-780 directly (Fig. 5I). These results further suggest that IR-780 can bind to SDHA protein directly, then to promote the inhibition of SDHA and SDH activity, but there may have other ways to downregulate SDHA by IR-780 besides directly binding and cleaving which need to be further investigated.

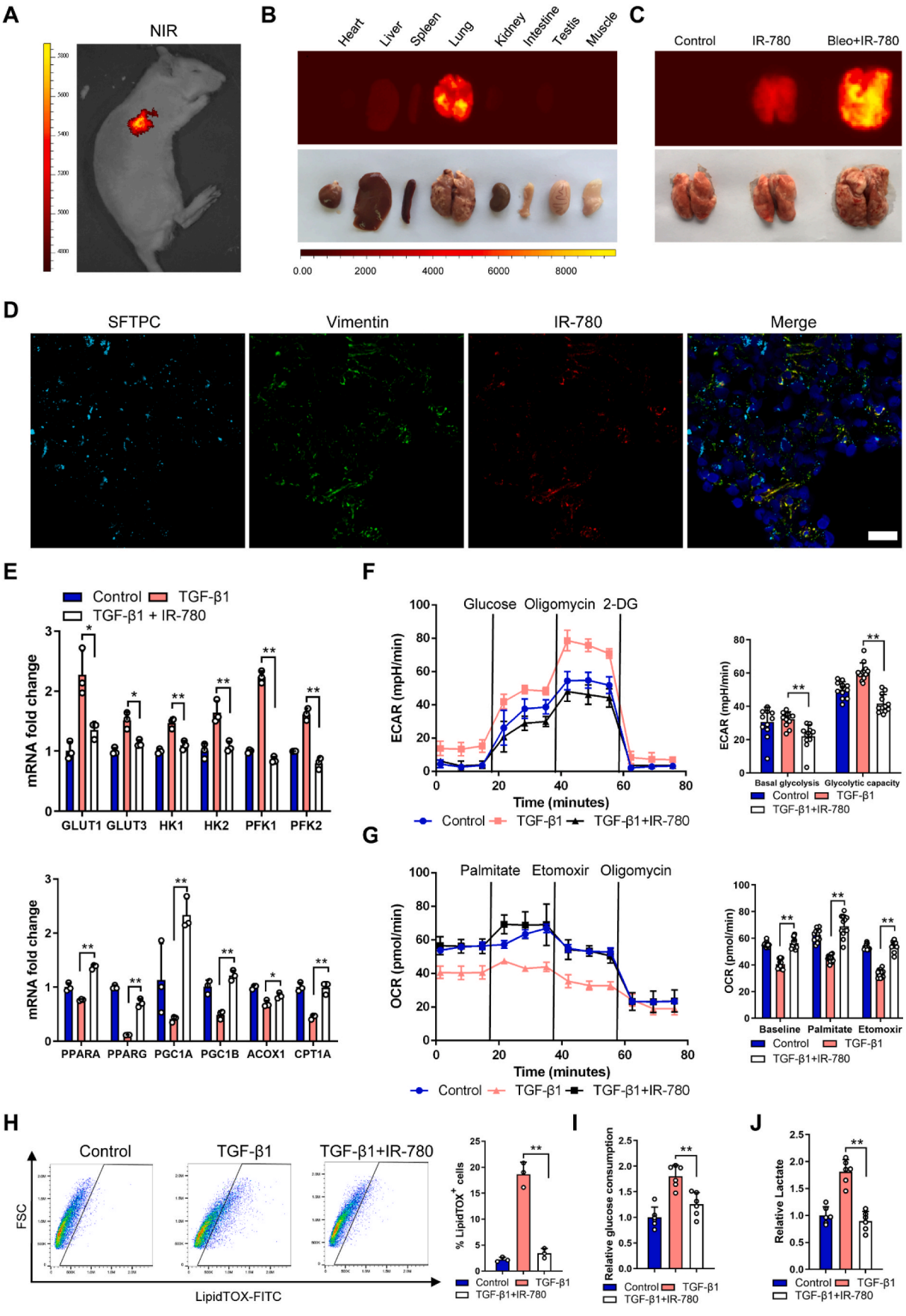

(caption on next page)

Fig. 4. IR-780 selectively accumulates into damaged lung tissues and inhibits glycolysis and promotes FAO. **A-B** The whole body NIR imaging and dissected organs of the bleomycin-treated rat following administrated IR-780. **C** The NIR fluorescent imaging further confirmed that IR-780 can preferentially accumulate into damaged lung tissues compared with healthy lung. **D** Representative image showing SFTPC (cyan), vimentin (green), IR-780 (red) and nuclei (blue) in rat lung tissue sample. The yellow is a mixture of red (IR-780) and green (Vimentin) in the merged picture. **E** qRT-PCR (n = 3) analysis of FAO and glycolysis mRNA levels in primary lung fibroblasts treated with or without TGF-β1 and IR-780 for 12 h (n = 3). **F-G** ECR and OCR in primary lung fibroblasts treated with or without TGF-β1 and IR-780 for 24 h (n = 4). ECAR, prior to glucose injection, is referred to as non-glycolytic acidification which is caused by other processes rather than glycolysis, and glucose-induced response is reported as the rate of glycolysis under basal conditions. **H** Gating strategy for detecting LipidTOX $^{+}$ cells by flow cytometry and quantification of LipidTOX $^{+}$ cell abundance in primary lung fibroblasts treated with or without TGF-β1 and IR-780 for 72 h (n = 3). **I-J** Glucose consumption and lactate abundance in primary lung fibroblast treated with or without TGF-β1 and IR-780 for 24 h (n = 6). Drug doses: TGF-β1 (5 ng/ml), IR-780 (0.5 μM). Bars represent 25 μm **(D)**. The results are presented as the means ± S.D. (**P < 0.01; One-way ANOVA). (For interpretation of the references to color in this figure legend, the reader is referred to the Web version of this article.)

2.5. IR-780 prevents bleomycin-induced lung fibrosis and respiratory dysfunction

Further, to understand whether IR-780 can improve fibrotic remodeling and is effective in attenuating lung fibrosis, IR-780 was intraperitoneally administered every 4 days after bleomycin instillation (Fig. 6A). Using RT-qPCR, we found IR-780 significantly upregulated FAO and downregulated glycolysis mRNA levels (Fig. S5A) as well as myofibroblast parameters (Fig. S5B) in fibroblast from bleomycin-treated lung. Micro-CT analysis of bleomycin treated rats at day 28 showed a marked change in the lung density and increased parenchymal opacity compared to control and IR-780 treated mice (Fig. 6B). Morphologically, IR-780 treated rats had improved lung morphology, with less lung collapse and fibrous nodules (Fig. 6B). In addition, bleomycin enhanced lung inflammatory responses as well as destructed lung architecture with thickened alveolar septa and collapsed alveolar spaces, as evidenced by the histological evaluation (Fig. 6B). Masson's trichrome staining showed reduced collagen deposition in IR-780 treated group (Fig. 6C). Bleomycin-induced lungs are characterized by architectural tissue remodeling with the accumulation of collagen I, fibronectin and α-SMA (Fig. 6C). Similarly, IR-780 attenuated mRNA levels of TGF-β1, as well as other genes involved in fibrogenesis, such as CTGF, COL1A1, MMP2, α-SMA, fibronectin and PAI-1 in lung tissues (Fig. 6D). Hydroxyproline and collagen abundance in lungs were also decreased in IR-780 treated group (Fig. 6E and F). Moreover, IR-780 markedly reduced airway inflammation and neutrophil-derived MPO levels in the lungs (Fig. 6G–I), and significantly decreased the abundance of active TGF-β1 in BALF (Fig. 6J), a pro-fibrogenic factor critical for lung fibrosis initiation and perpetuation. PAS staining showed that secretion of mucin was higher in the bronchus in bleomycin-induced rats compared with control and IR-780 treatment (Fig. 6K). Rats receiving IR-780 alone had no observable effect on the lungs as compared to the lungs of the control mice, and the HE staining displayed that other organs (liver, spleen, heart, kidney, colon and muscle) of rats were not obvious affected after IR-780 treatment (Fig. S5C).

Next, we evaluated the role of IR-780 in respiratory dysfunction induced by bleomycin, pulmonary function tests were performed using a whole-body plethysmograph. We found a significant increase of respiratory rate, accompanied by a decrease in tidal volume, which results in a little inhibition of minute volume compared to control and IR-780 treated group (Figure 6L), and bleomycin enhanced rats to adopt the rapid and shallow pattern that is characteristic of advanced fibrotic lung disease. To observe the effects of IR-780 on survival, we used a higher dose of bleomycin (2 folds) that would generally be lethal. IR-780 resulted in a substantial survival benefit, with a significant reduction in mortality from 80 % in the bleomycin-induced group to 40 % in the IR-780 treated group (Figure 6M). This survival benefit suggests that IR-780 potentially limits the acute lung injury caused by high-dose bleomycin in addition to antifibrotic effects. Taken together, IR-780 prevents bleomycin-induced lung fibrosis and respiratory dysfunction effectively.

2.6. Glycolysis enhances cell retention of IR-780 via SLCO4A1

Interestingly, we observed that myofibroblasts (TGF-β1 induced) showed significantly enhanced the fluorescence intensity of IR-780 (Fig. 7A and B). Considering the downregulation of FAO and upregulation of glycolysis in myofibroblast, myofibroblasts were treated with PPARA agonist (fenofibrate) or glycolysis inhibitor (2-DG, BAY876 and 3-PO), respectively. As shown in Fig. 7C, glycolysis inhibitors significantly decreased the cellular uptake of IR-780, while fenofibrate did not, suggesting glycolysis enhanced cell retention of IR-780. We have reported that OATPs (organic-anion-transporting polypeptide), also known as solute carrier organic anion (SLCO), are the carriers of IR-780 [45,46], but the main OATP which induce IR-780 uptake varies in different tissues or cell types. Notably, the accumulation of IR-780 in myofibroblasts was significantly decreased when administered the OATPs inhibitor BSP (bromosulfophthalein) (Fig. 7D). At the same time, IR-780 fluorescence intensity was also inhibited in normal fibroblasts when treated with BSP (Fig. S6A). Furthermore, we analyzed the GSE44723 dataset containing human fibroblasts from donor samples (4 cases of non-fibrotic individuals and 4 rapid progressing pulmonary fibrosis patient) [47], 6 members in solute carrier family (SLC) were upregulated, among them, only SLCO4A1 belongs to OATPs family (Fig. 7E and F). Western blot and RT-PCR confirmed that SLCO4A1 were significantly upregulated in myofibroblast (TGF-β1 induced) (Fig. 7G). Similarly, levels of SLCO4A1 were also increased in fibroblasts from fibrotic lung tissues (Fig. S6B). Further, SLCO4A1 siRNA significantly affected the IR-780 uptake in normal fibroblast (Fig. S6C) and myofibroblast (Fig. 7H). Considering HIF-1α are responsible for upregulation glycolysis in myofibroblast and HIF-1α was reported to directly regulate the SLCO superfamily [48], further studies indicated that HIF-1α mediated the upregulation of SLCO4A1 and uptake of IR-780 by using α-KG to inhibit HIF-1α (Fig. 7G and H). These data demonstrated that the uptake of IR-780 varies between fibroblast and myofibroblast in a HIF-1α/SLCO4A1 dependent manner and glycolysis enhanced cell retention of IR-780 via SLCO4A1.

2.7. Targeting apoptosis of myofibroblasts with IR-780 improves established fibrosis

Furthermore, IR-780 was demonstrated to efficiently decrease the cell viability of myofibroblast (TGF-β1 induced) when compared to normal fibroblast (Fig. 8A and Fig. S7A). Similarly, IR-780 rapidly induced the increase of total and mitochondrial superoxide both in primary normal fibroblast and myofibroblast, the ROS of fibroblast gradually declined to normal, but remained significantly elevated in myofibroblast (Fig. 8B and C). Mitochondrial complex II inhibition has been reported to maximize ROS production [49–51], and we found a severe inhibition of SDHA protein and SDH activity in IR-780 treated myofibroblast while normal fibroblast showed a mild and partial inhibition of SDHA protein level (Fig. S7B) and SDH activity (Fig. 8D). Then, the ability of promoting ROS production induced by IR-780 was suppressed in myofibroblast transfected with SDHA expressing plasmid (Fig. S7C), suggesting that SDHA inhibition is involved in the ROS generation induced by IR-780. Further, the promotion of apoptosis induced by IR-780 in myofibroblasts can be reversed by SLCO4A1 inhibition, NAC (a ROS inhibitor) treatment (Fig. 8E) and SDHA overexpression (Fig. S7D), indicating excessive uptake of IR-780 induced by

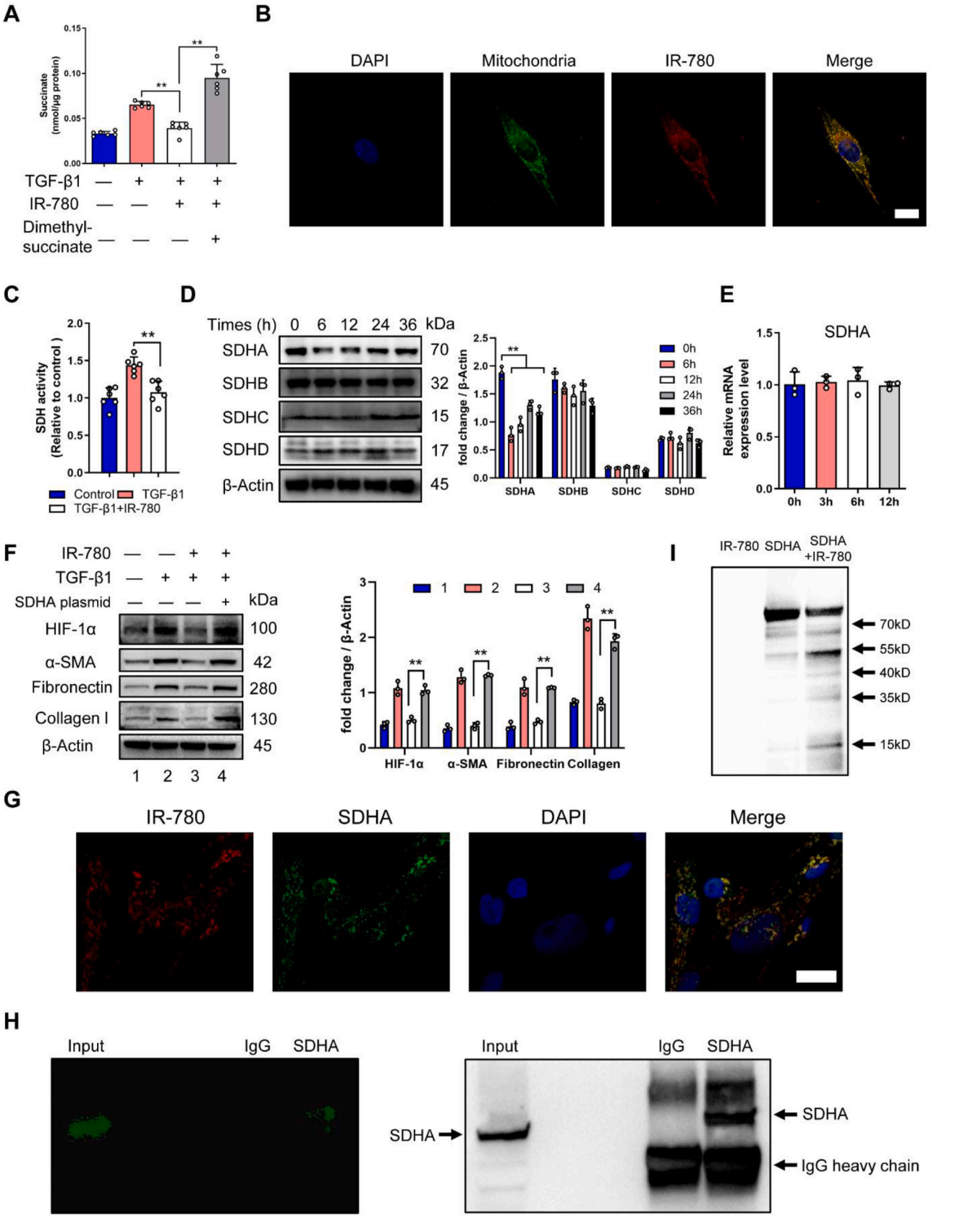

(caption on next page)

Fig. 5. IR-780 inhibits succinate accumulation by targeting succinate dehydrogenase subunit A (SDHA). **A** Succinate abundance in primary lung fibroblasts treated with or without TGF-β1, IR-780 and dimethyl succinate for 24 h (n = 6). **B** The subcellular localization of IR-780 and mitochondria in primary lung fibroblasts. **C** Succinate dehydrogenase (SDH) activity in primary lung fibroblasts treated with or without TGF-β1 and IR-780 for 24 h (n = 6). Cells were incubated with 0.5 μM IR-780 (no serum) for 10 min at 37 °C in the dark, after removing free dye, cells were cultured in fresh complete medium for the following experiments. **D** Western blot analysis of SDH subunits protein in primary lung fibroblasts treated with IR-780 for the indicated times. **E** mRNA level of SDHA in primary lung fibroblast treated with IR-780 for the indicated times. **F** Western blot analysis of SDHA, HIF-1α and profibrotic proteins in primary lung fibroblast transfected with or without SDHA expressing plasmid. **G** Representative image showing SDHA (green), IR-780 (red) and nuclei (blue) of primary lung fibroblast. **H** Pulldown assay was performed using SDHA antibody in the IR-780 treated primary lung fibroblasts lysates and showed that SDHA antibody could pull down proteins labeled with IR-780. **I** Western blot analysis of recombinant human SDHA protein treated with IR-780 in 4 °C overnight. Drug doses: TGF-β1 (5 ng/ml), IR-780 (0.5 μM), Dimethyl succinate (5 mM). Bars represent 25 μm **(B)**, 50 μm **(G)**. The results are presented as the means ± S.D. (**P < 0.01; One-way ANOVA). (For interpretation of the references to color in this figure legend, the reader is referred to the Web version of this article.)

SLCO4A1 and excessive ROS induced by severe inhibition of SDHA may contribute to myofibroblast apoptosis. We also observed swollen mitochondria and disappeared mitochondria ridges using transmission electron microscopy (TEM) in IR-780 treated myofibroblast (Fig. 8F).

Based on the above, we hypothesize that IR-780 can be beneficial in improving established fibrosis by targeting apoptosis of myofibroblasts. We examined the effects of delayed IR-780 treatment, that is, after 3 weeks of bleomycin injury for up to an additional 5 weeks (Fig. 8G). IR-780 promotes fibrosis resolution even after delayed exposure as demonstrated by Micro-CT analysis, morphology and HE staining (Fig. 8H). In addition, IR-780 significantly inhibits collagen deposition and α-SMA expression in lung tissues assessed by Masson's trichrome and immunofluorescent staining, respectively (Fig. 8I). Similarly, hydroxyproline and collagen abundance were decreased in IR-780 treated group (Fig. 8J and K). Moreover, IR-780 significantly decreased the abundance of active TGF-β1 in BALF and neutrophil-derived MPO levels in lung tissues (Fig. 8L–M), indicating less inflammation. Therefore, targeting apoptosis of myofibroblasts with IR-780 improves established lung fibrosis by inducing severe inhibition of succinate dehydrogenase and resulting in excessive ROS in myofibroblasts.

3. Discussion

Metabolomics has been applied to respiratory diseases such as cystic fibrosis, asthma and chronic obstructive pulmonary disease [52–55]. Meanwhile, IPF is associated with metabolic dysregulation [56] and IPF lungs display alterations in metabolic pathways for energy consumption during lung structural reconstruction, which may contribute to IPF pathogenesis [57]. One study has reported that type 2 diabetes mellitus might be a risk factor for either the initiation or progression of IPF [58] and fludeoxyglucose (FDG) uptake is found to be elevated in patients with IPF [59]. Several types of lipid molecules from plasma are identified as biomarkers for IPF [60]. However, whether these metabolic abnormalities (glucose and lipid metabolism) represent a cause or consequence of IPF remains unclear. In this study, we demonstrate that there is an upregulation of glycolysis and downregulation of fatty acid oxidation (FAO) in fibroblast from fibrotic lung, with higher lipid accumulation and triglyceride abundance in myofibroblast and fibrotic lung. At a cellular level, metabolic regulation was demonstrated to be a major driver of fibroblast transition. We demonstrated that suppression of FAO and promotion of glycolysis resulted in an elevation of myofibroblast parameters; conversely, by using PPARA agonist and glycolysis inhibitor, respectively, inhibited fibroblast transdifferentiation. Excess lipid accumulation has been proposed to promote the development of fibrosis and lipotoxicity [17]. However, our results suggest that higher intracellular lipid accumulation alone was not enough to induce profibrotic markers when cells are overexpressed CD36 and that substrate (fatty acid) uptake may not a limiting factor for lung fibrosis.

Succinate is an important metabolite of several metabolic pathways and plays a vital role in inflammation, endocrine and paracrine modulation, signal transduction and tumorigenesis [61]. In ischemia-reperfusion injury, ischemic accumulation of succinate controls reperfusion injury through mitochondrial ROS [34]. Succinate is elevated in inflammation and sustains IL-1β production [28]. We demonstrate that the accumulation of succinate both in fibrotic lung and myofibroblast, via fumarate production and reversal of SDH, is a universal metabolic signature in lung fibrosis; in turn, excess succinate can disrupt PHD activity, leading to the stabilization and activation of HIF-1α, then to cause upregulation of glycolysis and downregulation of FAO and promote the development of lung fibrosis. Thus, accumulation of succinate may be of further relevance via its role in fibrosis. These data demonstrate that succinate contributes to metabolic dysregulation in fibroblasts, and the inhibition of succinate accumulation or SDH activity is protective in preventing fibrosis formation.

SDH possesses bi-directional catalysis function in the process of succinate to fumarate. In most physiological conditions, SDH can reduce succinate to fumarate, and SDH inhibition can promote succinate accumulation and fumarate downregulation. However, under certain conditions (such as ischemia and hypoxia), SDH operates in reverse and reduce fumarate to succinate, and SDH inhibition reduces succinate abundance [31–34]. In this study, we suggest for the first time that SDH can act in reverse to promote the production of succinate in lung fibrosis, and the supply of fumarate may come from the pathways which had been proved by Chouchani et al. [34]. The bi-directional catalysis function of SDH was also characterized in liver fibrosis. It has been reported that succinate can accumulate in the liver fibrosis in mice fed a high-fat diet (HFD), and SDH can promote the accumulation of succinate [62], but in another study, SDH inhibition can increase succinate abundance which contributes to pro-fibrotic effects in hepatic stellate cells [63,64]. Therefore, we hypothesize that the function of SDH is different in various conditions or pathological process, but the detailed mechanism still needs further investigation.

Despite there are two FDA-approved drugs to treat IPF, pirfenidone act as a TGFβ1 inhibitor and nintedanib is a multi-receptor tyrosine kinase inhibitor, which cannot stop the progression of lung fibrosis completely. On the other hand, there is a lack of pharmaceutical agents to target the fibroblast metabolic dysregulation. We identified a NIR small molecule dye, IR-780, as a targeting agent, which can suppress glycolysis and promote FAO by mild inhibiting SDHA in fibroblasts, then prevent the formation of lung fibrosis. In our recently published research, we also identified that IR-780 can alleviate radiation-induced acute lung injury and fibrosis [65], suggesting broad-spectrum anti--fibrotic activity of IR-780. Considering the complexity and particularity of radiation-induced lung fibrosis, the bleomycin-induced pulmonary fibrosis, a most widely utilized and characterized model [66,67], was used to further investigate the detailed mechanism of IR-780 in mitigating lung fibrosis in this study. Moreover, persistent myofibroblast activation distinguishes pathological fibrosis from physiological wound healing, suggesting that therapies selectively inducing myofibroblast apoptosis could prevent progression and potentially improve established lung fibrosis. Consistent with our previous research that IR-780 can characterize HIF-1/glycolysis hyperactive cell population [68,69], we also identify that glycolysis enhances cell retention of IR-780 and may lead to severe inhibition of SDHA and excessive ROS in myofibroblasts, this offers the opportunity to successfully improve pulmonary fibrosis with IR-780 by targeting myofibroblasts apoptosis. To our knowledge, this is the first study to realize the prevention and treatment of lung fibrosis by suppressing SDH or SDHA with varying degrees in fibroblasts

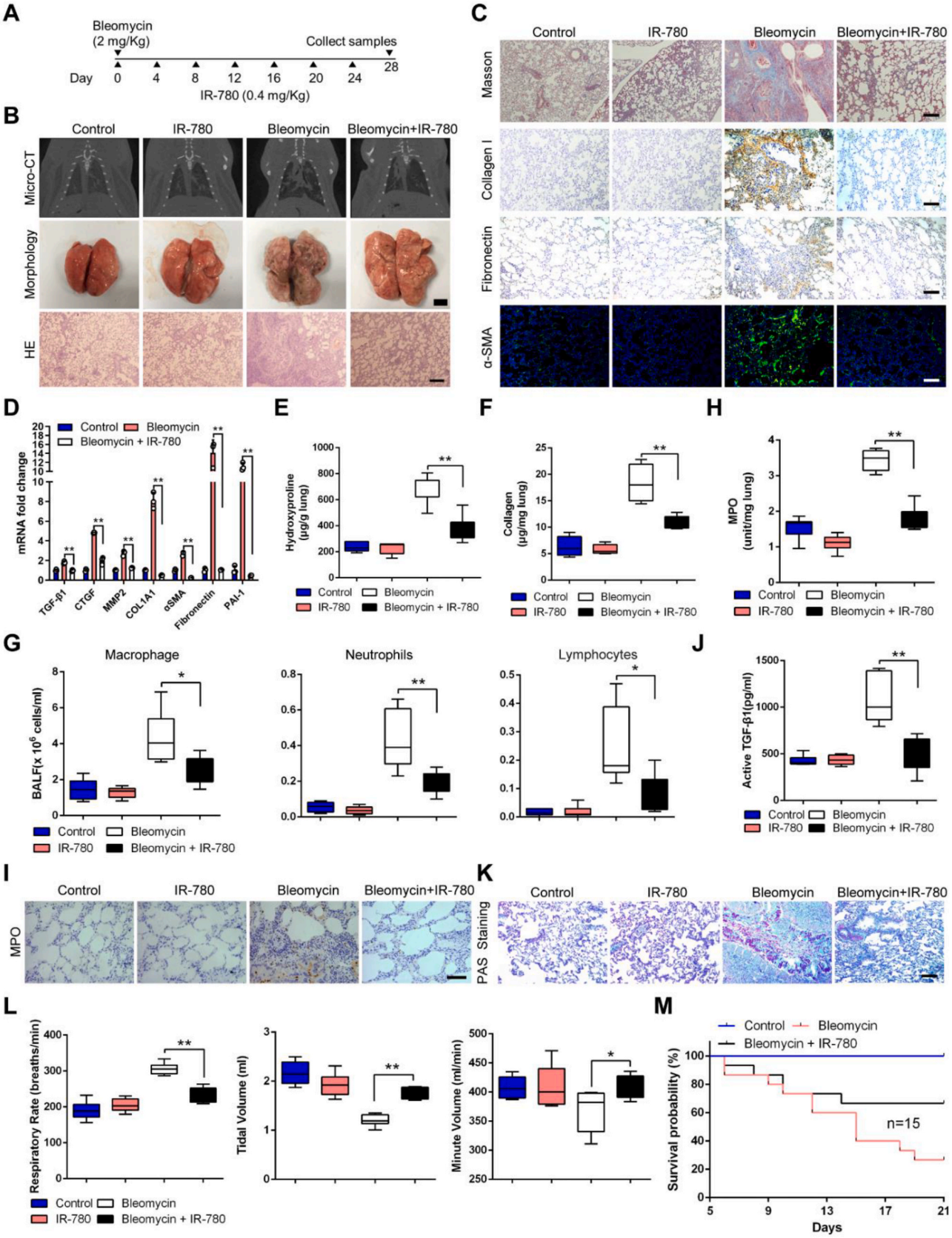

(caption on next page)

Fig. 6. IR-780 prevents bleomycin-induced lung fibrosis and respiratory dysfunction. **A** Protocol for bleomycin-induced lung injury, elicited by intratracheal instillation of 2 mg/kg bleomycin, and treatment regimen with intraperitoneal injection of 0.4 mg/kg IR-780 every 4 days. **B** Representative images of axial slices of reconstructed anatomical X-ray micro-CT images obtained at 28 days post treatment, bleomycin treated rats show parenchymal opacity (top); representative images showing gross lung morphology of rats (middle); representative photomicrographs of hematoxylin and eosin-stained lung sections (bottom). **C** Representative images of Masson's trichrome stained lung sections at 28 days post treatment; Immunohistochemistry analysis of representative rat lung tissue samples showing collagen I and fibronectin; Representative images showing α-SMA (green) and nuclei (blue) in lung sections. **D** qRT-PCR analysis of profibrotic mRNA levels from indicated lung tissues (n = 3). **E-F** Hydroxyproline abundance (n = 6 for control and IR-780 groups, n = 7 for bleomycin and bleomycin + IR-780 groups) and collagen abundance (n = 12) in the rat lung tissues indicated. **G** Quantification of macrophages, neutrophils, and lymphocytes abundance in BALF indicated (n = 6). **H** Analysis of myeloperoxidase (MPO) abundance in the lung tissues indicated (n = 12). **I** Immunohistochemistry analysis of representative rat lung tissue samples showing MPO. **J** Measurement of active levels of TGF-β1 in BALF indicated (n = 6). **K** Analysis of lung sections stained with periodic acid-Schiff (PAS). **L** Analysis of the respiratory rate, tidal volume, and minute volume (n = 6). **M** Survival curves of rats treated as indicated following intratracheal challenge with a double dose of bleomycin (4 mg/kg) or saline (n = 15). Bars represent 5 mm **(B, morphology)**, 250 μm **(B, HE)**, 250 μm **(C)**, 5 μm **(I)**, 250 μm **(K)**. The results are presented as the means ± S.D. (*p < 0.05, **P < 0.01; One-way ANOVA). (For interpretation of the references to color in this figure legend, the reader is referred to the Web version of this article.)

and myofibroblasts, respectively. This gives us a time for reflection and renewal that regulate metabolism can be a preventive strategy, meaningfully, we can also take advantage of the property of metabolic dysregulated cells to achieve the therapeutic effect. Hence, it is possible to control the occurrence and development of the disease by using just one agent, and IR-780 has broad implications for the management of lung fibrosis.

IR-780 can induce excessive ROS production in myofibroblasts at least by inhibiting SDHA, however, the mechanism of severe inhibition of SDHA and excessive ROS induced by IR-780 remains to be clarified which is possibly associated with enhanced cell retention of IR-780 via SLCO4A1 in myofibroblasts. Our previous work reported that IR-780 and its derivatives can induce excessive ROS in cancer cells by inhibiting mitochondrial complex I, II, V [44,70] and mitochondrial protein translocase [71], which also may play a potential role in excessive ROS of myofibroblasts although we primarily focused on the role of complex II. On the other hand, the mechanism of IR-780 in normal fibroblasts also needed to be further investigated. In this study, we found a severe inhibition of SDHA protein and SDH activity in IR-780 treated myofibroblast, while normal fibroblast showed a mild and partial inhibition of SDHA protein level and SDH activity which almost back to normal level after 24 h, this kind of phenomenon may be related to various cell retention of drug abundance and low concentrations of the drug in cells account for weak Drug/Mitochondria protein interactions which are not sufficient to promote apoptosis or cytotoxicity [72]. Further, IR-61, an IR-780 derivative, also provoked a transient release of mitochondrial and cytosolic superoxide, but the elevated ROS levels quickly reverted to normal levels because IR-61 can evoke the intracellular antioxidant defense mechanisms subsequently [73], and the similar role of IR-780 in normal lung fibroblast also needs us to verify.

Besides, inflammation are important triggers for fibrosis, and activated fibroblast also can secret a series of pro-inflammatory factors and pro-fibrotic proteins which attract inflammatory cells and contribute the lung inflammation [74]. However, the proposed mechanism of anti-fibrotic by IR-780 can be not well reconciled with anti-inflammatory effects, and further research is needed to investigate the detailed mechanism of regulating inflammation and fibroblasts. Meanwhile, faster proliferation could associate with many of the metabolic differences, glycolysis meets the metabolic requirements of cell proliferation and plays a fundamental role in supporting cell growth, and faster proliferation also could account for many of the metabolic differences [16]. Therefore, proliferation, metabolic and pro-fibrotic phenotype play important roles in the development of lung fibrosis. As expected, we found glycolytic inhibitors and IR-780 could downregulate the proliferation of TGF-β1 induced fibroblasts compared with normal fibroblasts. And in our study, we focused on the function of IR-780 in regulating fibroblast metabolic and pro-fibrotic phenotype, the mechanism of regulating cell proliferation by IR-780 need to be further investigated.

In summary, our studies suggest that upregulation of glycolysis and downregulation of FAO contribute to lung fibrosis formation, and this process is caused by a significant accumulation of succinate in fibroblasts. Therefore, succinate dehydrogenase is an exciting new therapeutic target to treat IPF, and IR-780 can be a promising agent to control lung fibrosis by targeting succinate dehydrogenase (Fig. 9).

4. Materials and methods

4.1. Animals

Male Sprague-Dawley (SD) rats (8–9 weeks) were purchased from Laboratory Animal Center of Third Military Medical University (Army Medical University, AMU). All experiments were conducted in accordance with the Guidelines for the Care and Use of Laboratory Animals of the AMU, and all procedures were approved by the Animal Care and Use Committee of the AMU.

4.2. Experimental models of lung fibrosis

For bleomycin administration, rats were anaesthetized with 0.1 % pentobarbital followed by intratracheal instillation of bleomycin (2 mg/kg) in 200 μl PBS. IR-780 (0.5 mg/kg) was prepared freshly at the time of administration by dissolving in 500 μl sterile PBS. Rats received the first dose of IR-780 (0.5 mg/kg, i.p.) or DMM (40 mg/kg, i.p.) immediately after bleomycin treatment. IR-780 (0.5 mg/kg, i.p.) was then administered every 4 days, DMM (40 mg/kg, i.p.) was then administered every day for 14 days. All rats were killed 28 days after bleomycin treatment, the lungs and other organs were harvested for further analysis. Further experiments were designed to measure the effects of delayed IR-780 administration. IR-780 (1 mg/kg, i.p.) treatment was initiated 3 weeks after exposure to bleomycin, and rats received IR-780 every 4 days for 5 weeks.

4.3. Reagents and antibodies

Recombinant TGF-β1 and recombinant PDGF-BB were purchased from PEPROTECH. α-ketoglutarate (α-KG), IR-780, dimethyl malonate (DMM), dimethyl succinate and aminooxyacetate (AOA) were obtained from Sigma-Aldrich. Fenofibrate, sodium succinate, glucose and oligomycin were purchased from Selleck. 2-DG, BAY876, 3-PO, etomoxir, bleomycin, AICAR and vigabatrin were obtained from MCE. Palmitate-conjugated BSA was purchased from Seahorse Bioscience. Oil Red O was from Nanjing Jiancheng Bio-engineering.

Antibodies to GLUT1 (AB_10837075), GLUT3 (AB_10694437), PFK1 (AB_10996606), PPARA (AB_2252506), PPARG (AB_10596794), PGC1A (AB_2828002), PGC1B (AB_2879093), ACOX1 (AB_2221670), CPT1A (AB_2084676), α-SMA (AB_2223009), fibronectin (AB_2105691), Collagen I (AB_2082037), β-Actin (AB_2687938), SDHA (AB_11182164), SDHB (AB_2285522), SDHC (AB_2183291), SLCO4A1 (AB_2880501), HK1 (AB_2878162), PFK2 (AB_2162854), SDHD (AB_2880540), anti-CD36 (AB_10597244) were purchased from Proteintech. Antibodies to HIF-1α (AB_296474), HK2 (AB_2868547) were obtained from Abcam (The number inside the brackets is the Research Resource Identifier (RRID) of antibody). Secondary antibodies to

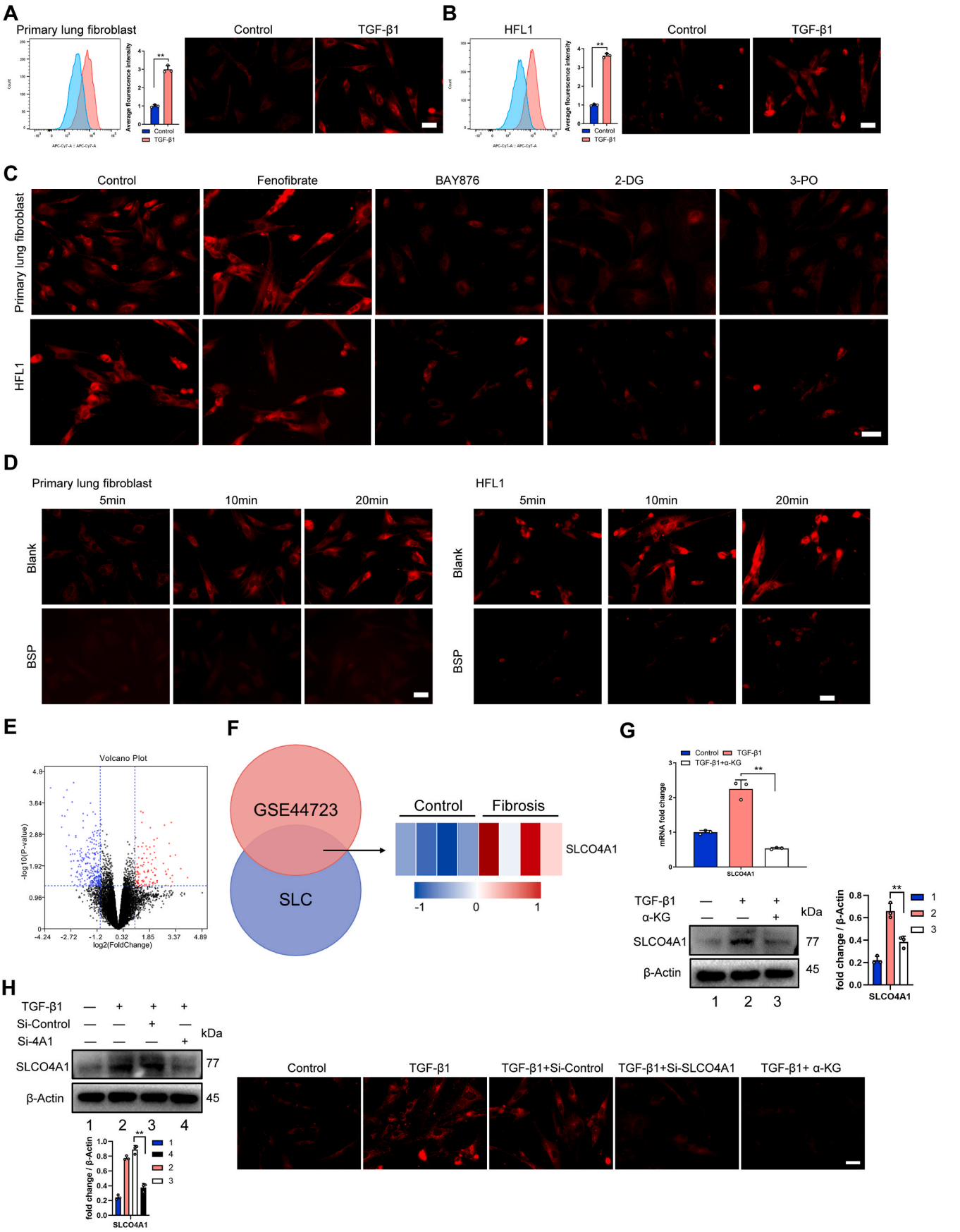

(caption on next page)

Fig. 7. Glycolysis enhances cell retention of IR-780 via SLCO4A1. **A-B** Cellular IR-780 uptake was detected by flow cytometry (left). Quantification of average fluorescence intensity (middle). Representative images showing accumulation of IR-780 in lung fibroblasts (right). Cells were incubated with 0.5 μM IR-780 for 10 min at 37 °C in the dark, after removing free dye, cells were harvested for flow cytometry to detect fluorescence intensity. **C-D** Testing the effects of PPARA agonist (fenofibrate), glycolytic inhibitors (BAY876, 2-DG, 3PO) and OATPs inhibitor (BSP) on the uptake of IR-780 in myofibroblast (TGF-β1 induced). Cells were incubated with 0.5 μM IR-780 for 10 min at 37 °C in the dark, after removing free dye, the fluorescence of IR-780 was observed and images were captured by using a fluorescent microscope. **E** Volcano plots showing the results of genomic profiling of RNA from the GSE44723 dataset. The red or blue dots represent genes that are significantly ($P < 0.05$) up-regulated or down-regulated, respectively ($n = 4$ in each group); **F** Venn diagram showing that solute carrier family (SLC) genes and upregulated genes in GSE44723 shared 6 significantly upregulated SLC genes in rapid progressing pulmonary fibrosis compared with non-fibrotic individuals ($P < 0.05$ by *t*-test; fold change>2) (left). Heat map of genomic profiling of RNA showing the up-regulated SLCO4A1 ($P < 0.05$ by *t*-test; fold change>2) (right). **G** Relative mRNA ($n = 3$) and protein levels of SLCO4A1 in HFL1 treated with or without TGF-β1 and α-KG. **H** Representative immunoblots of the expressions of SLCO4A1 in control HFL1 or cells knockdown of SLCO4A1 (left). Representative images showing accumulation of IR-780 in HFL1 of indicated group (right). Drug doses: TGF-β1 (5 ng/ml), IR-780 (0.5 μM), BAY-876 (2.5 μM), 3-PO (5 mM), 2-DG (5 mM), fenofibrate (1 μM), BSP (250 μM), α-KG (1 mM). Bars represent 250 μm **(A-D and H)**. The results are presented as the means ± S.D. (**$P < 0.01$; A and B, student's t-test; G, One-way ANOVA). (For interpretation of the references to color in this figure legend, the reader is referred to the Web version of this article.)

different species IgG of Alexa Fluor® 594 (red) or 488 (green) were purchased from Invitrogen. DAPI and Hoechst 33342 were obtained from Beyotime.

4.4. Cell isolation and culture

Primary rat lung fibroblasts were isolated from new-born SD rat. Fibroblasts from healthy and fibrotic lung were isolated from SD rats after 28 days of PBS or bleomycin treatment. Rat lungs were perfused with PBS. Lungs were then washed with ice-cold HBSS-Ca/Mg and lungs tissues were minced with sterilized scissors. Minced tissues were then incubated on shaker at 37 °C for 1 h with digestion buffer (0.3 mg/ml type IV collagenase and 0.5 mg/ml trypsin dissolved in HBSS-Ca/Mg). Digested tissues were then passed through 40-μm cell strainer. Cells were centrifuged at 800 rpm for 5 min, and cell pellets were resuspended in growth medium (F12K containing 10 % FBS, 1 % streptomycin/penicillin) and seeded in a culture plate. Since fibroblast cells are known to attach very fast in comparison with epithelial cells, seeded cells were left to attach for 2–4 h. Next, cultured plates were washed with PBS and a fresh growth medium was added. Human fetal lung fibroblast 1 (HFL1) was purchased from ATCC and maintained in F12K growth medium (Gibco) supplemented with 10 % fetal bovine serum and 1 % streptomycin/penicillin. Cells were grown in a 5 % CO_2 atmosphere at 37 °C.

For IR-780 pre-treated group, cells were incubated with 0.5 μM or 1 μM IR-780 (no serum) for 10 min at 37 °C in the dark. After removing free dye, cells were washed twice with PBS, and cultured in fresh complete medium for following experiment. α-KG, DMM, dimethyl succinate, AOA, fenofibrate, sodium succinate, 2-DG, BAY876, 3-PO, etomoxir, AICAR and vigabatrin were pretreated for 12 h in advance, and were kept in the medium for the following experiment. All mRNA and protein profiling were performed 12 h and 24 h post treatment, respectively. For TGF-β1 induced myofibroblast, cells were treated with TGF-β1 for 72 h, and cultured in fresh complete medium for the following experiment (kept with TGF-β1).

4.5. Near-infrared fluorescent (NIR) imaging

For in vivo NIR imaging, rats were tail vein injection with IR-780 at a dose of 0.5 mg/kg 24 h later, rats were anaesthetized by intra-abdominal injection of 1 % pentobarbital sodium and the whole body NIR fluorescent imaging was taken using a Kodak In-Vivo FX Profession Imaging System equipped with fluorescent filter sets (excitation/emission, 770/830 nm). All the settings were applied as described previously [75]. To further study the lung accumulation property of IR-780, lungs and important internal organs in the rat were isolated and obtained for NIR fluorescent imaging at the day of animal sacrifice.

4.6. Staining for lipid-droplet accumulation

Cultured primary lung fibroblasts were washed with PBS. A mixture of diluted LipidTOX (1:200) and Hoechst 33342 (1:5000) in PBS was then used to stain cells. Subsequently, lipid-droplet imaged by confocal microscopy.

4.7. Triglyceride measurement

Lung triglyceride was measured using quantification kits (Nanjing Jiancheng Bio-engineering) according to the manufacturer's instructions.

4.8. Glucose consumption assay

Cells were seeded in culture plates for 12 h. The culture medium was then changed, and cells were incubated for 24 h. Glucose in medium was measured according to the manufacturer's instructions using a Glucose Colorimetric Assay Kit (Cayman Chemical).

4.9. FAO and glycolysis functional assessment for lung fibroblast

Seahorse experiments were performed on an XFe96 analyzer (Aligent) according to the manufacturer's instructions. Lung fibroblast were plated on an XF96 culture plate. For glycolysis profiling, a final concentration of 10 mM glucose, 1 μM oligomycin, and 100 mM 2-DG were used. For FAO, 170 μM palmitate-conjugated BSA, 40 μM Etomoxir and 2 μM oligomycin were used.

4.10. Pull-down assay

Primary lung fibroblasts were incubated with 0.5 μM of IR-780 for 10 min. After washed with PBS, total proteins were extracted using ice-cold RIPA buffer containing protease inhibitor cocktail (Roche). The protein lysate was incubated with SDHA antibody overnight at 4 °C. Then, 25 μl of Pierce Protein A/G Magnetic Beads (Thermo) was added for 1 h at room temperature. After collect the beads using a magnetic stand, the protein complex was analyzed by SDS-PAGE and imaging to determine whether SDHA combined with the NIR fluorescence small-molecule IR-780, then immunoblotted using anti-SDHA antibody.

4.11. LC-MS/MS analysis of excised gel bands

To isolate potential interacted proteins for LC-MS/MS analysis, human fetal lung fibroblast cell lines (HFL1) were incubated with 0.5 μM of IR-780 for 10 min. After washed with PBS, total proteins were extracted for SDS-PAGE. Taking advantage of the NIR fluorescent property of IR-780, the NIR fluorescent gel tapes were scooped out under the NIR imaging guide, the NIR-labeled proteins were extracted and subjected to LC-MS/MS analysis.

4.12. Western blot analysis

Total proteins were extracted, the concentrations were determined using a BCA kit (Beyotime). Equal amount of protein from each sample

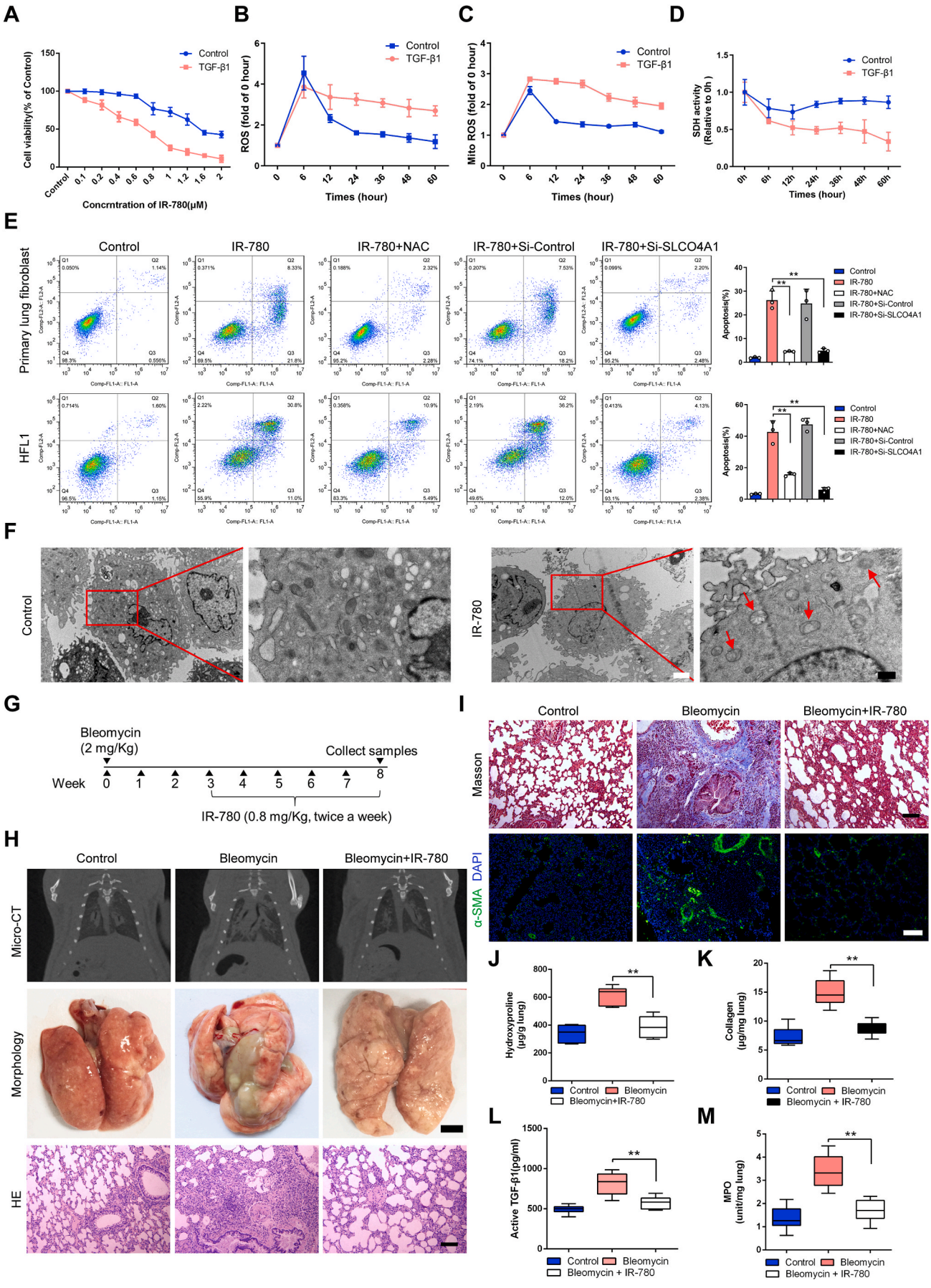

(caption on next page)

Fig. 8. Targeting apoptosis of myofibroblasts with IR-780 improves established fibrosis. **A** Cells were incubated with different concentration of IR-780 (no serum) for 10 min at 37 °C in the dark, after removing free dye, cells were cultured in fresh complete medium for 48 h to detect the killing effect by using CCK-8 (n = 6). For TGF-β1 induced myofibroblast, cells were treated with TGF-β1 (5 ng/ml) for 72 h and cultured in fresh complete medium for the following experiment (kept with TGF-β1). **B-C** Reactive oxygen species (ROS) and mitochondrial superoxide levels in fibroblast of indicated groups (n = 3). **D** Succinate dehydrogenase (SDH) activity in fibroblast of indicated groups (n = 6). **E** Myofibroblasts were incubated with 1 μM IR-780 (no serum) for 10 min at 37 °C in the dark and cultured in fresh complete medium for 48 h to detect apoptosis by using flow cytometry (left). Quantification of apoptosis (right) (n = 3). **F** Myofibroblasts were incubated with 1 μM IR-780 (no serum) for 10 min at 37 °C in the dark and cultured in fresh complete medium for 48 h to observe mitochondria by using transmission electron microscopy. **G** Protocol for bleomycin-induced lung injury, elicited by intratracheal instillation of 2 mg/kg bleomycin, and treatment regimen with intraperitoneal injection of 0.8 mg/kg IR-780 twice a week. **H** Representative images of axial slices of reconstructed anatomical X-ray micro-CT images obtained at 8 weeks post treatment (top); representative images showing gross lung morphology of rats (middle); representative photomicrographs of hematoxylin and eosin-stained lung sections (bottom). **I** Representative images of Masson's trichrome stained lung sections at 8 weeks post treatment; Representative images showing α-SMA (green) and nuclei (blue) in lung sections. **J-K** Hydroxyproline (n = 6) and collagen abundance (n = 12) in the rat lung tissues indicated. **L** Measurement of active levels of TGF-β1 in BALF (n = 6). **M** Analysis of myeloperoxidase (MPO) expression in the lungs (n = 12). Bars represent 2 μm **(F, white)**, 0.5 μm **(F, black)**, 5 mm **(H, morphology)**, 250 μm **(H, HE)**, 250 μm **(I)**. The results are presented as the means ± S.D. (**P < 0.01; One-way ANOVA). (For interpretation of the references to color in this figure legend, the reader is referred to the Web version of this article.)

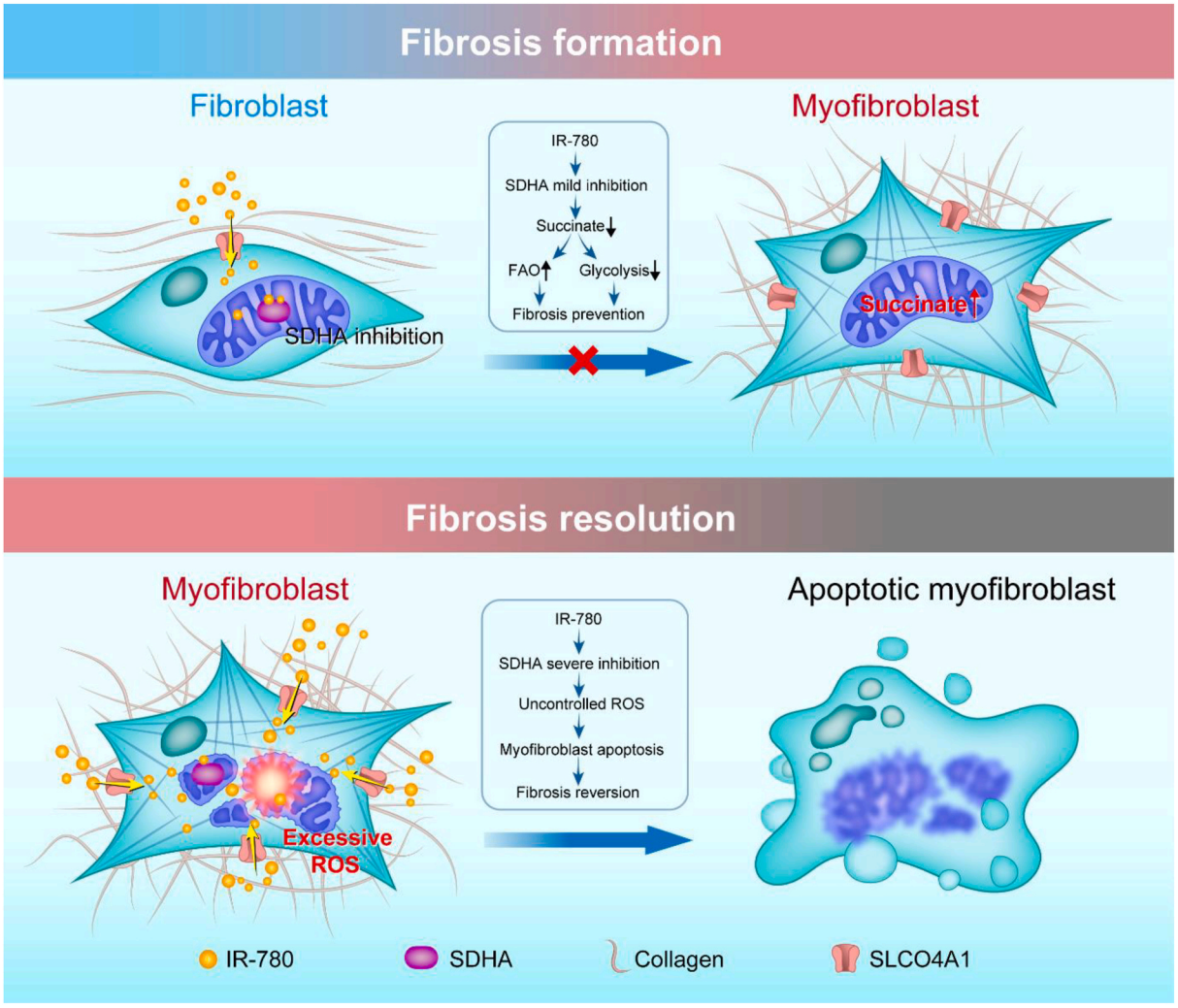

Fig. 9. Proposed model of targeting succinate dehydrogenase of fibroblasts by IR-780 controls bleomycin induced lung fibrosis. Glycolysis upregulation and FAO downregulation contribute to lung fibrosis formation, and this process is caused by a significant accumulation of succinate in fibroblasts. IR-780, a near-infrared small molecule dye, as a targeting agent which stimulates mild inhibition of succinate dehydrogenase subunit A (SDHA) in normal fibroblasts, and which inhibits TGF-β1 induced SDH and succinate elevation, then to prevent fibrosis formation and respiratory dysfunction. Furthermore, enhanced cell retention of IR-780 at least partially mediating by SLCO4A1 is shown to promote severe inhibition of SDHA in myofibroblasts, which may contribute to excessive ROS generation and selectively induces myofibroblasts to apoptosis, and then therapeutically improves established lung fibrosis in vivo.

was run in 8–12 % Tris-glycine SDS-PAGE gel, followed by transfer to PVDF membrane (Millipore). Membranes were blocked with Quick-block™Blocking buffer (Beyotime) for 30 min and probed with primary antibodies at 4 °C overnight, followed by incubation with horseradish peroxidase-conjugated anti-IgG (Beyotime) for 1 h at 37 °C. The intensity of bands was visualized and determined using an enhanced chemiluminescence detection system (Bio-Rad Laboratories).

4.13. Quantitative real-time PCR analysis

RNA was isolated from harvested cells using RNeasy Micro Kit (QIAGEN). cDNA synthesis was done following the manufacturer protocol (Maxima First Strand cDNA Synthesis Kit, Thermo Scientific, K1671). For mitochondrial DNA level determination, DNA was purificated using the KingFisher Cell and Tissue DNA Kit (Thermo). Real-time PCR was performed using a SYBR Green qPCR master mix (Takara) according to the manufacturer's protocol. The primers for the qRT-PCR are listed in Supplementary Table 1. All data were normalized to the control using Actin or RPLPO as internal control.

4.14. Cell toxicity and proliferation

The effect of IR-780 on the proliferation of lung fibroblasts was assessed using a cell viability assay (Cell Counting Kit-8 (CCK-8); Dojindo Molecular Technologies, Inc., Japan). Briefly, cells were seeded in 96-well plates at an initial density of 5×10^3 cells/well for 12 h and pretreated with different concentration of IR-780 for 10 min at 37 °C in the dark. Then, cells were cultured in 100 μL fresh complete medium for 48 h and assessed using the CCK-8. The absorbance of the samples was measured at 450 nm.

4.15. RNA interference, plasmid, and retroviral vectors transfection

After cells were grown to 40–50 % confluence, cells were transfected with small interfering RNAs (siRNA, GenePharma), negative control RNA (NC siRNA, GenePharma) or SDHA expressing plasmid (Genechem) with Lipofectamine 3000 (Invitrogen) according to manufacturer's instructions. CD36 overexpressed lentiviral vectors and control lentiviral vectors were obtained from Genechem and transfected into HFL1 following the manufacturer's instructions. Fresh culture medium was added to cultures after 12 h post-transfection. Transfected cells for other experiments were performed 24 h post-transfection. The siRNAs for RNA interference are listed in Supplementary Table 2.

4.16. Flow cytometry

Cells were subjected to flow cytometry using Accuri C6 (BD Biosciences). For lipid-droplet analysis, cultured fibroblasts were washed with PBS and resuspended in PBS containing LipidTOX (1:200). Then cells were subjected to flow cytometry following incubation for 30 min. For analysis of ROS, H2DCF-DA (Beyotime) and MitoSOX Red mitochondrial superoxide indicator (Molecular Probes) were used to measure the intracellular ROS and Mitochondrial superoxide according to the manufacturer's instructions. For apoptosis analysis, cells were washed twice with cold PBS, resuspended in binding buffer, and incubated with annexin-V and PI (BD Biosciences) for 15 min at room temperature in the dark. After incubation, cells were analyzed by flow cytometry.

4.17. Hydroxyproline assays

Lung hydroxyproline abundance was analyzed using a hydroxyproline colorimetric assay kit from Biovision following the manufacturer's instructions.

4.18. Total collagen assay

Lung collagen abundance was assessed using Sircol™ Soluble Collagen Assay (Biocolor) according to the manufacturer's instructions.

4.19. Determination of lactate, succinate dehydrogenase (SDH), malate, AMP, fumarate, NADH/NAD+ and succinate

Lactate production (Lactate Assay Kit) in lung tissues or medium were measured as described by the manufacturer (BioVision). Succinate dehydrogenase (SDH), malate, AMP, fumarate and succinate assay kit were purchased from Abcam and were measured according to the instructions.

4.20. Lung histology and imaging

Formalin-fixed, paraffin-embedded lung sections stained with PAS (Abcam) and optimal cutting temperature compound (OCT)-embedded frozen sections for Oil Red O staining. Immunocytochemistry and immunohistochemistry were used on paraformaldehyde-fixed cells and formalin-fixed, paraffin-embedded lung sections. Slides were then incubated with the primary antibody overnight at 4 °C, followed by a 1.5 h incubation with the secondary antibody. Then nuclei were stained with DAPI. Images were captured using fluorescent microscope (Olympus BX51).

4.21. Transmission electron microscopy

Cells were harvested and immediately fixed in 2.5 % glutaraldehyde overnight at 4 °C and post-fixed with 2 % osmium tetroxide for 1 h at 37 °C. Subsequently, cells were embedded and stained using uranylacetate/lead citrate. The sections were imaged using a TEM (JEM-1400PLUS, Japan).

4.22. Statistical analysis

All data are presented as means ± standard deviations. Statistical analyses were applied using the unpaired Student's t-test or one-way ANOVA (Bonferroni) analysis of variance to determine statistical significance. Asterisks denote statistical significance (*$P < 0.05$; **$P < 0.01$). Statistical analyses were carried out using the SPSS 13.0 package (SPSS Inc., Chicago, IL, USA).

4.23. Data availability

The authors declare that all data supporting the findings of this study are available within the paper and its Supplementary Information files, and from the authors on request.

Acknowledgments

This work was supported by the Key Program of National Natural Science Foundation of China (82030056) and the National Key Research and Development Program (2016YFC1000805), and University Innovation Team Building Program of Chongqing (CXTDG201602020), and intramural research project grants (AWS17J007, and 2018-JCJQ-ZQ-001).

Appendix A. Supplementary data

Supplementary data to this article can be found online at https://doi.org/10.1016/j.redox.2021.102082.

Author contributions

Z.W., L.C. and Y.H. contributed equally to this work. C.S and Z.W. designed, carried out and analyzed data from most of the experiments and wrote the manuscript with input from all co-authors; L.C., Y.H., M. L., H.W. and Z.J. performed the experiments. J.Z., Z.Y., Z.C. and C.Z. conceived and supervised the study. L.L., Ya.W, X.L., F.L., Y.G., P.L., Y. L., Yu.W., X.T., Z.Z, and A.Z analyzed and interpreted data from experiments; all authors discussed the results and commented on the manuscript.

Declaration of competing interest

The authors declare no competing interest.

References

[1] H.M. Al-Tamari, S. Dabral, A. Schmall, P. Sarvari, C. Ruppert, J. Paik, R. A. DePinho, F. Grimminger, O. Eickelberg, A. Guenther, W. Seeger, R. Savai, S. S. Pullamsetti, FoxO3 an important player in fibrogenesis and therapeutic target for idiopathic pulmonary fibrosis, EMBO Mol. Med. 10 (2) (2018) 276–293.

[2] G. Sgalla, A. Biffi, L. Richeldi, Idiopathic pulmonary fibrosis: diagnosis, epidemiology and natural history, Respirology 21 (3) (2016) 427–437.

[3] P.M. George, A.U. Wells, R.G. Jenkins, Pulmonary fibrosis and COVID-19: the potential role for antifibrotic therapy, the Lancet, Respir. Med. 8 (8) (2020) 807–815.

[4] V. Kheirollahi, R.M. Wasnick, V. Biasin, A.I. Vazquez-Armendariz, X. Chu, A. Moiseenko, A. Weiss, J. Wilhelm, J.S. Zhang, G. Kwapiszewska, S. Herold, R. T. Schermuly, B. Mari, X. Li, W. Seeger, A. Gunther, S. Bellusci, E. El Agha, Metformin induces lipogenic differentiation in myofibroblasts to reverse lung fibrosis, Nat. Commun. 10 (1) (2019) 2987.

[5] S. Rangarajan, N.B. Bone, A.A. Zmijewska, S. Jiang, D.W. Park, K. Bernard, M. L. Locy, S. Ravi, J. Deshane, R.B. Mannon, E. Abraham, V. Darley-Usmar, V. J. Thannickal, J.W. Zmijewski, Metformin reverses established lung fibrosis in a bleomycin model, Nat. Med. 24 (8) (2018) 1121–1127.

[6] J. Milara, A. Serrano, T. Peiro, A. Gavalda, M. Miralpeix, E.J. Morcillo, J. Cortijo, Aclidinium inhibits human lung fibroblast to myofibroblast transition, Thorax 67 (3) (2012) 229–237.

[7] X. Zhao, J.Y.Y. Kwan, K. Yip, P.P. Liu, F.F. Liu, Targeting metabolic dysregulation for fibrosis therapy, Nat. Rev. Drug Discov. 19 (1) (2020) 57–75.

[8] H. Zhu, W. Chen, D. Liu, H. Luo, The role of metabolism in the pathogenesis of systemic sclerosis, Metab. Clin. Exp. 93 (2019) 44–51.

[9] R.J. DeBerardinis, C.B. Thompson, Cellular metabolism and disease: what do metabolic outliers teach us? Cell 148 (6) (2012) 1132–1144.

[10] M.G. Vander Heiden, L.C. Cantley, C.B. Thompson, Understanding the Warburg effect: the metabolic requirements of cell proliferation, Science 324 (5930) (2009) 1029–1033.

[11] B. Kelly, L.A. O'Neill, Metabolic reprogramming in macrophages and dendritic cells in innate immunity, Cell Res. 25 (7) (2015) 771–784.

[12] M. Black, D. Milewski, T. Le, X. Ren, Y. Xu, V.V. Kalinichenko, T.V. Kalin, FOXF1 inhibits pulmonary fibrosis by preventing CDH2-CDH11 cadherin switch in myofibroblasts, Cell Rep. 23 (2) (2018) 442–458.

[13] B. Hinz, S.H. Phan, V.J. Thannickal, A. Galli, M.L. Bochaton-Piallat, G. Gabbiani, The myofibroblast: one function, multiple origins, Am. J. Pathol. 170 (6) (2007) 1807–1816.

[14] H.M. Kok, L.L. Falke, R. Goldschmeding, T.Q. Nguyen, Targeting CTGF, EGF and PDGF pathways to prevent progression of kidney disease, Nat. Rev. Nephrol. 10 (12) (2014) 700–711.

[15] D.F. Higgins, M.P. Biju, Y. Akai, A. Wutz, R.S. Johnson, V.H. Haase, Hypoxic induction of Ctgf is directly mediated by Hif-1, Am. J. Physiol. Renal 287 (6) (2004) F1223–F1232.

[16] S.Y. Lunt, M.G. Vander Heiden, Aerobic glycolysis: meeting the metabolic requirements of cell proliferation, Annu. Rev. Cell Dev. Biol. 27 (2011) 441–464.

[17] I.J. Goldberg, C.M. Trent, P.C. Schulze, Lipid metabolism and toxicity in the heart, Cell Metabol. 15 (6) (2012) 805–812.

[18] K. Susztak, E. Ciccone, P. McCue, K. Sharma, E.P. Bottinger, Multiple metabolic hits converge on CD36 as novel mediator of tubular epithelial apoptosis in diabetic nephropathy, PLoS Med. 2 (2) (2005) 152–161.

[19] X. Zhao, P. Psarianos, L.S. Ghoraie, K. Yip, D. Goldstein, R. Gilbert, I. Witterick, H. Pang, A. Hussain, J.H. Lee, J. Williams, S.V. Bratman, L. Ailles, B. Haibe-Kains, F.-F. Liu, Metabolic regulation of dermal fibroblasts contributes to skin extracellular matrix homeostasis and fibrosis, Nat. Metabol. 1 (1) (2019) 147–157.

[20] D.F. Higgins, K. Kimura, M. Iwano, V.H. Haase, Hypoxia-inducible factor signaling in the development of tissue fibrosis, Cell Cycle 7 (9) (2008) 1128–1132.

[21] Z. Lokmic, J. Musyoka, T.D. Hewitson, I.A. Darby, Hypoxia and hypoxia signaling in tissue repair and fibrosis, Int. Rev. Cell Mol. Biol. 296 (2012) 139–185.

[22] J. Goodwin, H. Choi, M.H. Hsieh, M.L. Neugent, J.M. Ahn, H.N. Hayenga, P. K. Singh, D.B. Shackelford, I.K. Lee, V. Shulaev, S. Dhar, N. Takeda, J.W. Kim, Targeting hypoxia-inducible factor-1alpha/pyruvate dehydrogenase kinase 1 Axis by dichloroacetate suppresses bleomycin-induced pulmonary fibrosis, Am. J. Respir. Cell Mol. Biol. 58 (2) (2018) 216–231.

[23] J.W. Kim, I. Tchernyshyov, G.L. Semenza, C.V. Dang, HIF-1-mediated expression of pyruvate dehydrogenase kinase: a metabolic switch required for cellular adaptation to hypoxia, Cell Metabol. 3 (3) (2006) 177–185.

[24] H. Lu, R.A. Forbes, A. Verma, Hypoxia-inducible factor 1 activation by aerobic glycolysis implicates the Warburg effect in carcinogenesis, J. Biol. Chem. 277 (26) (2002) 23111–23115.

[25] S.J. Yeung, J. Pan, M.H. Lee, Roles of p53, MYC and HIF-1 in regulating glycolysis - the seventh hallmark of cancer, Cell. Mol. Life Sci. 65 (24) (2008) 3981–3999.

[26] D. Huang, T.T. Li, X.H. Li, L. Zhang, L.C. Sun, X.P. He, X.Y. Zhong, D.Y. Jia, L. B. Song, G.L. Semenza, P. Gao, H.F. Zhang, HIF-1-Mediated suppression of acyl-CoA dehydrogenases and fatty acid oxidation is critical for cancer progression, Cell Rep. 8 (6) (2014) 1930–1942.

[27] W. Du, L. Zhang, A. Brett-Morris, B. Aguila, J. Kerner, C.L. Hoppel, M. Puchowicz, D. Serra, L. Herrero, B.I. Rini, S. Campbell, S.M. Welford, HIF drives lipid deposition and cancer in ccRCC via repression of fatty acid metabolism, Nat. Commun. 8 (1) (2017) 1769.

[28] G.M. Tannahill, A.M. Curtis, J. Adamik, E.M. Palsson-McDermott, A.F. McGettrick, G. Goel, C. Frezza, N.J. Bernard, B. Kelly, N.H. Foley, L. Zheng, A. Gardet, Z. Tong, S.S. Jany, S.C. Corr, M. Haneklaus, B.E. Caffrey, K. Pierce, S. Walmsley, F. C. Beasley, E. Cummins, V. Nizet, M. Whyte, C.T. Taylor, H. Lin, S.L. Masters, E. Gottlieb, V.P. Kelly, C. Clish, P.E. Auron, R.J. Xavier, L.A.J. O'Neill, Succinate is an inflammatory signal that induces IL-1 beta through HIF-1 alpha, Nature 496 (7444) (2013) 238–+.

[29] M.A. Selak, S.M. Armour, E.D. MacKenzie, H. Boulahbel, D.G. Watson, K. D. Mansfield, Y. Pan, M.C. Simon, C.B. Thompson, E. Gottlieb, Succinate links TCA cycle dysfunction to oncogenesis by inhibiting HIF-alpha prolyl hydroxylase, Canc. Cell 7 (1) (2005) 77–85.

[30] A.C. Smith, A.J. Robinson, A metabolic model of the mitochondrion and its use in modelling diseases of the tricarboxylic acid cycle, BMC Syst. Biol. 5 (2011).

[31] Z.V. Niatsetskaya, S.A. Sosunov, D. Matsiukevich, I.V. Utkina-Sosunova, V. I. Ratner, A.A. Starkov, V.S. Ten, The oxygen free radicals originating from mitochondrial complex I contribute to oxidative brain injury following hypoxia-ischemia in neonatal mice, J. Neurosci. : Off. J. Soc. Neurosci. 32 (9) (2012) 3235–3244.

[32] H. Taegtmeyer, Metabolic responses to cardiac hypoxia. Increased production of succinate by rabbit papillary muscles, Circ. Res. 43 (5) (1978) 808–815.

[33] P.W. Hochachka, K.B. Storey, Metabolic consequences of diving in animals and man, Science 187 (4177) (1975) 613–621.

[34] E.T. Chouchani, V.R. Pell, E. Gaude, D. Aksentijevic, S.Y. Sundier, E.L. Robb, A. Logan, S.M. Nadtochiy, E.N.J. Ord, A.C. Smith, F. Eyassu, R. Shirley, C.H. Hu, A. J. Dare, A.M. James, S. Rogatti, R.C. Hartley, S. Eaton, A.S.H. Costa, P.S. Brookes, S.M. Davidson, M.R. Duchen, K. Saeb-Parsy, M.J. Shattock, A.J. Robinson, L. M. Work, C. Frezza, T. Krieg, M.P. Murphy, Ischaemic accumulation of succinate controls reperfusion injury through mitochondrial ROS, Nature 515 (7527) (2014) 431–435.

[35] E. Easlon, F. Tsang, C. Skinner, C. Wang, S.J. Lin, The malate-aspartate NADH shuttle components are novel metabolic longevity regulators required for calorie restriction-mediated life span extension in yeast, Genes Dev. 22 (7) (2008) 931–944.

[36] J.T. Barron, L. Gu, J.E. Parrillo, Malate-aspartate shuttle, cytoplasmic NADH redox potential, and energetics in vascular smooth muscle, J. Mol. Cell. Cardiol. 30 (8) (1998) 1571–1579.

[37] G. Van den Berghe, M.F. Vincent, J. Jaeken, Inborn errors of the purine nucleotide cycle: adenylosuccinase deficiency, J. Inherit. Metab. Dis. 20 (2) (1997) 193–202.

[38] V. Sridharan, J. Guichard, C.Y. Li, R. Muise-Helmericks, C.C. Beeson, G.L. Wright, O(2)-sensing signal cascade: clamping of O(2) respiration, reduced ATP utilization, and inducible fumarate respiration, American journal of physiology, Cell Physiol. 295 (1) (2008) C29–C37.

[39] Y.H. Huang, J. Zhou, S.L. Luo, Y. Wang, J.T. He, P. Luo, Z.L. Chen, T. Liu, X. Tan, J. J. Ou, H.M. Miao, H.J. Liang, C.M. Shi, Identification of a fluorescent small-molecule enhancer for therapeutic autophagy in colorectal cancer by targeting mitochondrial protein translocase TIM44, Gut 67 (2) (2018) 307–319.

[40] A.L. Vahrmeijer, M. Hutteman, J.R. van der Vorst, C.J.H. van de Velde, J. V. Frangioni, Image-guided cancer surgery using near-infrared fluorescence, Nat. Rev. Clin. Oncol. 10 (9) (2013) 507–518.

[41] A.L. Antaris, H. Chen, K. Cheng, Y. Sun, G.S. Hong, C.R. Qu, S. Diao, Z.X. Deng, X. M. Hu, B. Zhang, X.D. Zhang, O.K. Yaghi, Z.R. Alamparambil, X.C. Hong, Z. Cheng, H.J. Dai, A small-molecule dye for NIR-II imaging, Nat. Mater. 15 (2) (2016) 235–+.

[42] C. Zhang, L. Long, C. Shi, Mitochondria-targeting IR-780 dye and its derivatives: synthesis, mechanisms of action, and theranostic applications, Adv. Therapeut. 1 (7) (2018), 1800069.

[43] Y. Wang, T. Liu, E. Zhang, S. Luo, X. Tan, C. Shi, Preferential accumulation of the near infrared heptamethine dye IR-780 in the mitochondria of drug-resistant lung cancer cells, Biomaterials 35 (13) (2014) 4116–4124.

[44] Y. Wang, S.L. Luo, C. Zhang, X.Y. Liao, T. Liu, Z.Y. Jiang, D.Q. Liu, X. Tan, L. Long, Y. Wang, Z.L. Chen, Y.S. Liu, F. Yang, Y.B. Gan, C.M. Shi, An NIR-fluorophore-based therapeutic endoplasmic reticulum stress inducer, Adv. Mater. 30 (33) (2018).

[45] Z.L. Chen, Z.W. Wang, T.T. Jin, G.F. Shen, Y. Wang, X. Tan, Y.B. Gan, F. Yang, Y. S. Liu, C.J. Huang, Y.X. Zhang, X.B. Fu, C.M. Shi, Fibrogenic fibroblast-selective near-infrared phototherapy to control scarring, Theranostics 9 (23) (2019) 6797–6808.

[46] E.L. Zhang, S.L. Luo, X. Tan, C.M. Shi, Mechanistic study of IR-780 dye as a potential tumor targeting and drug delivery agent, Biomaterials 35 (2) (2014) 771–778.

[47] R.Q. Peng, S. Sridhar, G. Tyagi, J.E. Phillips, R. Garrido, P. Harris, L. Burns, L. Renteria, J. Woods, L. Chen, J. Allard, P. Ravindran, H. Bitter, Z.M. Liang, C. M. Hogaboam, C. Kitson, D.C. Budd, J.S. Fine, C.M.T. Bauer, C.S. Stevenson, Bleomycin induces molecular changes directly relevant to idiopathic pulmonary fibrosis: a model for "active" disease, PloS One 8 (4) (2013).

[48] J.B. Wu, C. Shao, X. Li, C. Shi, Q. Li, P. Hu, Y.T. Chen, X. Dou, D. Sahu, W. Li, H. Harada, Y. Zhang, R. Wang, H.E. Zhau, L.W. Chung, Near-infrared fluorescence imaging of cancer mediated by tumor hypoxia and HIF1alpha/OATPs signaling axis, Biomaterials 35 (28) (2014) 8175–8185.

[49] L. Bleier, S. Drose, Superoxide generation by complex III: from mechanistic rationales to functional consequences, Biochim. Biophys. Acta 1827 (11–12) (2013) 1320–1331.

[50] S. Drose, U. Brandt, The mechanism of mitochondrial superoxide production by the cytochrome bc1 complex, J. Biol. Chem. 283 (31) (2008) 21649–21654.

[51] C.L. Quinlan, A.A. Gerencser, J.R. Treberg, M.D. Brand, The mechanism of superoxide production by the antimycin-inhibited mitochondrial Q-cycle, J. Biol. Chem. 286 (36) (2011) 31361–31372.
[52] S. Carraro, S. Rezzi, F. Reniero, K. Heberger, G. Giordano, S. Zanconato, C. Guillou, E. Baraldi, Metabolomics applied to exhaled breath condensate in childhood asthma, Am. J. Respir. Crit. Care Med. 175 (10) (2007) 986–990.
[53] Y.P. Kang, W.J. Lee, J.Y. Hong, S.B. Lee, J.H. Park, D. Kim, S. Park, C.S. Park, S. W. Park, S.W. Kwon, Novel approach for analysis of bronchoalveolar lavage fluid (BALF) using HPLC-QTOF-MS-based lipidomics: lipid levels in asthmatics and corticosteroid-treated asthmatic patients, J. Proteome Res. 13 (9) (2014) 3919–3929.
[54] D.J. Adamko, P. Nair, I. Mayers, R.T. Tsuyuki, S. Regush, B.H. Rowe, Metabolomic profiling of asthma and chronic obstructive pulmonary disease: a pilot study differentiating diseases, J. Allergy Clin. Immunol. 136 (3) (2015) 571–+.
[55] T.A. Laguna, C.S. Reilly, C.B. Williams, C. Welchlin, C.H. Wendt, Metabolomics analysis identifies novel plasma biomarkers of cystic fibrosis pulmonary exacerbation, Pediatr. Pulmonol. 50 (9) (2015) 869–877.
[56] N. Xie, Z. Tan, S. Banerjee, H. Cui, J. Ge, R.M. Liu, K. Bernard, V.J. Thannickal, G. Liu, Glycolytic reprogramming in myofibroblast differentiation and lung fibrosis, Am. J. Respir. Crit. Care Med. 192 (12) (2015) 1462–1474.
[57] Y.D. Zhao, L. Yin, S. Archer, C. Lu, G. Zhao, Y. Yao, L. Wu, M. Hsin, T.K. Waddell, S. Keshavjee, J. Granton, M. de Perrot, Metabolic heterogeneity of idiopathic pulmonary fibrosis: a metabolomic study, BMJ Open Respir. Res. 4 (1) (2017), e000183.
[58] M.C. Garcia-Sancho Figueroa, G. Carrillo, R. Perez-Padilla, M.R. Fernandez-Plata, I. Buendia-Roldan, M.H. Vargas, M. Selman, Risk factors for idiopathic pulmonary fibrosis in a Mexican population, Case-Contr. Stud., Respir. Med. 104 (2) (2010) 305–309.
[59] A. Justet, A. Laurent-Bellue, G. Thabut, A. Dieudonne, M.P. Debray, R. Borie, M. Aubier, R. Lebtahi, B. Crestani, [(18)F]FDG PET/CT predicts progression-free survival in patients with idiopathic pulmonary fibrosis, Respir. Res. 18 (1) (2017) 74.
[60] F. Yan, Z.S. Wen, R. Wang, W.L. Luo, Y.F. Du, W.J. Wang, X.Y. Chen, Identification of the lipid biomarkers from plasma in idiopathic pulmonary fibrosis by Lipidomics, BMC Pulm. Med. 17 (2017).
[61] E. Mills, L.A. O'Neill, Succinate: a metabolic signal in inflammation, Trends Cell Biol. 24 (5) (2014) 313–320.
[62] L. She, D. Xu, Z. Wang, Y. Zhang, Q. Wei, J. Aa, G. Wang, B. Liu, Y. Xie, Curcumin inhibits hepatic stellate cell activation via suppression of succinate-associated HIF-1alpha induction, Mol. Cell. Endocrinol. 476 (2018) 129–138.
[63] X.J. Liu, L. Xie, K. Du, C. Liu, N.P. Zhang, C.J. Gu, Y. Wang, M.F. Abdelmalek, W. Y. Dong, X.P. Liu, C. Niu, C. Yang, A.M. Diehl, J. Wu, Succinate-GPR-91 receptor signalling is responsible for nonalcoholic steatohepatitis-associated fibrosis: effects of DHA supplementation, Liver Int. : Off. J. Int. Assoc. Stud. Liver 40 (4) (2020) 830–843.
[64] Y.H. Li, S.H. Woo, D.H. Choi, E.H. Cho, Succinate causes alpha-SMA production through GPR91 activation in hepatic stellate cells, Biochem. Biophys. Res. Commun. 463 (4) (2015) 853–858.
[65] M. Luo, L. Chen, J. Zheng, Q. Wang, Y. Huang, F. Liao, Z. Jiang, C. Zhang, G. Shen, J. Wu, Y. Wang, Y. Wang, Y. Leng, S. Han, A. Zhang, Z. Wang, C. Shi, Mitigation of Radiation-Induced Pulmonary Fibrosis by Small-Molecule Dye IR-780, Free Radical Biology & Medicine, 2021.
[66] D. Lagares, A. Santos, P.E. Grasberger, F. Liu, C.K. Probst, R.A. Rahimi, N. Sakai, T. Kuehl, J. Ryan, P. Bhola, J. Montero, M. Kapoor, M. Baron, X. Varelas, D. J. Tschumperlin, A. Letai, A.M. Tager, Targeted apoptosis of myofibroblasts with the BH3 mimetic ABT-263 reverses established fibrosis, Sci. Transl. Med. 9 (420) (2017).
[67] G. Yu, A. Tzouvelekis, R. Wang, J.D. Herazo-Maya, G.H. Ibarra, A. Srivastava, J.P. W. de Castro, G. DeIuliis, F. Ahangari, T. Woolard, N. Aurelien, R. Arrojo e Drigo, Y. Gan, M. Graham, X. Liu, R.J. Homer, T.S. Scanlan, P. Mannam, P.J. Lee, E. L. Herzog, A.C. Bianco, N. Kaminski, Thyroid hormone inhibits lung fibrosis in mice by improving epithelial mitochondrial function, Nat. Med. 24 (1) (2017) 39–49.
[68] Y. Wang, X. Liao, J. Sun, B. Yi, S. Luo, T. Liu, X. Tan, D. Liu, Z. Chen, X. Wang, C. Shi, Characterization of HIF-1alpha/Glycolysis hyperactive cell population via small-molecule-based imaging of mitochondrial transporter activity, Adv. Sci. 5 (3) (2018), 1700392.
[69] Z. Chen, Z. Wang, T. Jin, G. Shen, Y. Wang, X. Tan, Y. Gan, F. Yang, Y. Liu, C. Huang, Y. Zhang, X. Fu, C. Shi, Fibrogenic fibroblast-selective near-infrared phototherapy to control scarring, Theranostics 9 (23) (2019) 6797–6808.
[70] C. Zhang, T. Liu, P. Luo, L. Gao, X. Liao, L. Ma, Z. Jiang, D. Liu, Z. Yang, Q. Jiang, Y. Wang, X. Tan, S. Luo, Y. Wang, C. Shi, Near-infrared oxidative phosphorylation inhibitor integrates acute myeloid leukemia-targeted imaging and therapy, Sci. Adv. 7 (1) (2021).
[71] Y. Huang, J. Zhou, S. Luo, Y. Wang, J. He, P. Luo, Z. Chen, T. Liu, X. Tan, J. Ou, H. Miao, H. Liang, C. Shi, Identification of a fluorescent small-molecule enhancer for therapeutic autophagy in colorectal cancer by targeting mitochondrial protein translocase TIM44, Gut 67 (2) (2018) 307–319.
[72] Y. Shi, S.K. Lim, Q. Liang, S.V. Iyer, H.Y. Wang, Z. Wang, X. Xie, D. Sun, Y.J. Chen, V. Tabar, P. Gutin, N. Williams, J.K. De Brabander, L.F. Parada, Gboxin is an oxidative phosphorylation inhibitor that targets glioblastoma, Nature 567 (7748) (2019) 341–346.
[73] X. Wang, Z. Chen, S. Luo, T. Jin, Y. Wang, F. Chen, L. Wu, X. Tan, C. Shi, Development of therapeutic small-molecule fluorophore for cell transplantation, Adv. Funct. Mater. 26 (46) (2016) 8397–8407.
[74] P. Heukels, C.C. Moor, J.H. von der Thusen, M.S. Wijsenbeek, M. Kool, Inflammation and immunity in IPF pathogenesis and treatment, Respir. Med. 147 (2019) 79–91.
[75] C. Zhang, T. Liu, Y. Su, S. Luo, Y. Zhu, X. Tan, S. Fan, L. Zhang, Y. Zhou, T. Cheng, C. Shi, A near-infrared fluorescent heptamethine indocyanine dye with preferential tumor accumulation for in vivo imaging, Biomaterials 31 (25) (2010) 6612–6617.